UNCLASSIFIED

AD NUMBER

AD813227

NEW LIMITATION CHANGE

TO

Approved for public release, distribution unlimited

FROM

Distribution authorized to U.S. Gov't. agencies and their contractors; Critical Technology; Mar 1967. Other requests shall be referred to Army Electronics Command, Attn: AMSEL-KL-TM, Fort Monmouth, NJ 07703.

AUTHORITY

USAAEC ltr, 16 Jun 1971

THIS PAGE IS UNCLASSIFIED

AD

AD 813227

TECHNICAL REPORT ECOM-01257-1

STUDY AND INVESTIGATION LEADING TO THE DESIGN OF BROADBAND HIGH POWER KLYSTRON AMPLIFIERS

FIRST TRIANNUAL

By

ERLING LIEN - DARRELL ROBINSON

MARCH, 1967

ECOM

UNITED STATES ARMY ELECTRONICS COMMAND • FORT MONMOUTH, N.J. 07703

CONTRACT DA 28-043 AMC 02157(E)

EIMAC

DIVISION OF VARIAN

301 Industrial Way

San Carlos, California

DISTRIBUTION STATEMENT

This document is subject to special export controls and each transmittal to foreign governments or foreign nationals may be made only with prior approval of CG, USAECOM, ATTN: AMSEL-KL-TM, Fort Monmouth, N.J. 07703

TECHNICAL REPORT ECOM-02157-1 MARCH, 1967

STUDY AND INVESTIGATION LEADING to the DESIGN OF BROADBAND HIGH-POWER KLYSTRON AMPLIFIERS

FIRST TRIANNUAL REPORT

10 August 1966 to 9 December 1966

Report No. 1

CONTRACT NO. DA 28-043 AMC-02157(E)

DA PROJECT NO. 1E6-22001-A-055-04-78

Prepared by

E. Lien and D. Robinson

EIMAC, Division of Varian

San Carlos, California

For

UNITED STATES ARMY ELECTRONICS COMMAND

Fort Monmouth, New Jersey 07703

DISTRIBUTION STATEMENT

This document is subject to special export controls and each transmittal to foreign governments or foreign nationals may be made only with prior approval of CG, USAECOM, ATTN: AMSEL-KL-TM, Fort Monmouth, New Jersey, 07703.

ABSTRACT

The purpose of this program is to investigate methods for improving the bandwidth capabilities of high-power klystron amplifiers. The objective is a 1 db bandwidth improvement of at least fifty percent over the current state of the art. Particular emphasis is being placed on the study of extended-interaction resonators, and the possible optimization of these resonators through the use of mode overlapping.

In this report, the results of the initial investigation into the effects of mode overlapping in extended-interaction resonators is presented. During the first four-month reporting period, this investigation has been primarily concerned with the influence of a number of different parameters on the interaction impedance, bandwidth, and frequency response of the resonators. The parameters of particular interest are: the coupling between the two cavities, the degree of external loading and the location of the external load, the beam synchronization parameter, and the relative frequencies of the two cavities. The initial analysis has been restricted to two-gap resonators.

It is shown theoretically that the bandwidth of extended-interaction resonators can be increased through the use of mode overlapping. Comparisons with the bandwidths of other types of resonators at a given maximum impedance level show that a two-gap extended-interaction resonator with mode overlapping can have a 1 db bandwidth advantage of approximately three to one over a two-gap,single-mode,extended-interaction resonator, and close to four to one over a conventional single-gap cavity. The bandwidth of a two-gap,single-section-filter loaded resonator is about the same as that of the two-gap, mode-overlapping resonator at a given impedance level.

ABSTRACT (Continued)

Three different lumped-element equivalent circuits were considered to represent coupled-cavity resonators. These circuits are compared with experimental cases and with each other. It is concluded that the most practical circuit to use is one in which the coupling between the cavities is represented by a single shunt circuit element.

FOREWORD

This document is a report of the work performed on Contract DA 28-043 AMC-02157(E) during the first four-month period.

The program is being carried out in the High Power Microwave Tube Laboratory. The principal engineers are Erling Lien, who is serving as project leader, and Darrell Robinson.

Sponsorship and direction of the program are from the U.S. Army Electronics Command, Fort Monmouth, New Jersey. The assigned Army Project Engineer is Park Richmond.

TABLE OF CONTENTS

Title Page i

Abstract ii

Foreword iv

List of Figures vii

INTRODUCTION 1

A. Purpose 1

B. Progress 2

TWO-GAP EXTENDED-INTERACTION RESONATORS WITH MODE OVERLAPPING 3

A. Introduction 3

B. Equivalent Circuit 5

C. Modes of the Undriven Resonator 7

D. Frequency Response of the Driven Resonator 12

E. Bandwidth Comparisons Between Different Resonator Types 35

INVESTIGATION OF TWO ADDITIONAL EQUIVALENT CIRCUITS TO REPRESENT COUPLED-CAVITY RESONATORS 41

A. Introduction 41

B. First Equivalent Circuit 42

1. Modes of the Lossless Circuit 44

2. R_{sh}/Q of the Circuit 45

3. Comparison with Experimental Cases 47

C. Second Equivalent Circuit 54

1. Modes of the Lossless Circuit 56

2. R_{sh}/Q of the Circuit 57

3. Comparison with Experimental Cases 58

TABLE OF CONTENTS (Continued)

INVESTIGATION OF TWO ADDITIONAL EQUIVALENT CIRCUITS TO REPRESENT COUPLED-CAVITY RESONATORS (Continued).....

D. Conclusions 59

CONCLUSIONS AND FUTURE PLANS 65

A. Introduction 65

B. Conclusions 65

C. Future Plans 66

REFERENCES 68

GLOSSARY OF SYMBOLS 70

APPENDIX --

I - Derivation of the Basic Equations Used in the Analysis of Two-Gap Extended-Interaction Resonators ... I - 1

DISTRIBUTION LIST

LIST OF FIGURES

Fig. 1 Inductively-coupled, two-gap resonator equivalent circuit 6

Fig. 2 RF gap voltage vectors in a two-gap resonator as a function of the coupling parameter α. V_1 is used for a reference 9

Fig. 3 RF gap voltage vectors in a two-gap resonator as a function of the loaded Q of the second cavity 10

Fig. 4 RF gap voltage vectors in a two-gap resonator. The loaded cavity is tuned low 13

Fig. 5 RF gap voltage vectors in a two-gap resonator. The loaded cavity is tuned high 14

Fig. 6 Power response of a two-gap driven resonator for different values of the coupling parameter α. The real part of the interaction impedance is proportional to the power 18

Fig. 7 Power response of the two-gap driven resonator for three different values of the beam synchronization parameter 20

Fig. 8 RF gap voltage and drive current vectors in the resonator of Fig. 6. $\alpha = 0.13$, $\omega/\omega_1 = 0.91$ 22

Fig. 9 RF gap voltage and drive current vectors in the resonator of Fig. 6. $\alpha = 0.13$, $\omega/\omega_1 = 0.94$ 23

Fig. 10 RF gap voltage and drive current vectors in the resonator of Fig. 6. $\alpha = 0.13$, $\omega/\omega_1 = 0.975$ 24

Fig. 11 RF gap voltage and drive current vectors in the resonator of Fig. 6, except cavity #1 loaded. The power response is the same as shown in Fig. 6. $\alpha = 0.13$, ω/ω_1, $= 0.91$ 25

Fig. 12 RF gap voltage and drive current vectors in the resonator of Fig. 6, except cavity #1 loaded. $\alpha = 0.13$, $\omega/\omega_1 = 0.94$ .. 26

Fig. 13 RF gap voltage and drive current vectors in the resonator of Fig. 6, except cavity #1 loaded. $\alpha = 0.13$, $\omega/\omega_1 = 0.975$. 27

Fig. 14 Power response of the driven two-gap resonator showing the effect of tuning the loaded cavity low while the other parameters are held constant 29

Fig. 15 Power response of the two-gap driven resonator with the loaded cavity tuned low and the beam synchronization parameter adjusted for equal power output in the two modes. $\gamma_2 = 0.98$, $\theta_2(\text{at } \omega_1) = -1.55\pi$ 30

LIST OF FIGURES (Continued)

Fig. 16 Power response of the two-gap driven resonator. The beam synchronization has been adjusted so $\theta_2 = -\pi$ at the lower frequency mode, and the loaded cavity has been tuned low to yield equal power output in the two modes 31

Fig. 17 RF gap voltage and drive current vectors in the resonator of Fig. 16. $\omega/\omega_1 = 0.88$ 32

Fig. 18 RF gap voltage and drive current vectors in the resonator of Fig. 16. $\omega/\omega_1 = 0.915$ 33

Fig. 19 RF gap voltage and drive current vectors in the resonator of Fig. 16. $\omega/\omega_1 = 0.945$ 34

Fig. 20 Two-gap resonator equivalent circuit with resonant coupling . 43

Fig. 21 Typical two-gap extended-interaction resonator 46

Fig. 22 Values of ω_π/ω_1 and $(R_{sh}/Q)_\pi$ predicted by the circuit of Fig. 20 as a function of the two coupling parameters ω_1/ω_s and L_s/L_1 52

Fig. 23 A second two-gap resonator equivalent circuit with resonant coupling 55

Fig. 24 Predicted power responses of a driven two-gap resonator as given by two different circuits. The mode separation in the lossless case is the same in both circuits 62

Fig. 25 A second comparison between the resonator power responses predicted by the two different circuits. The values of ω_1/ω_s and L_s/L_1 have been changed, but the mode separation in the lossless case is still the same as in Fig. 24 63

INTRODUCTION

A. Purpose

The purpose of this program is to investigate methods for improving the bandwidth capabilities of high-power klystron amplifiers. The objective is a 1 db bandwidth improvement of at least fifty percent over the current state of the art. This is to be achieved without undue degradation of gain or efficiency and without sacrificing stability. Particular emphasis is being placed on the study of extended-interaction resonators, and the possible optimization of these resonators through the use of mode overlapping.

The investigation is being carried out theoretically with the aid of equivalent circuits and mathematical models, and experimentally to the extent of performing cold-test measurements on the resonators. Where applicable, resonator parameters are chosen to be consistent with a design example of a 5 megawatt peak-power klystron. Specific design goals and tentative parameters chosen for this example klystron are listed below.

Frequency	5.5 GHz
Gain	35 db
Bandwidth (1db)	14%
Output power	5Mw
Efficiency	35%
Beam Voltage	140 kv
Beam Current	105 A
Perveance	2.0×10^{-6}

Beam current density	244 Amps/cm^2
Normalized beam radius, γb	0.54 rad.
Brillouin focusing field	1200 gauss
Normalized tunnel radius, γa	0.77 rad.
Normalized interaction gap length βed	1.2 rad.

B. Progress

Most of the work on this contract during the first reporting period was aimed at studying the effects of mode overlapping in two-gap extended-interaction resonators. One objective of this study was to arrive at general design criteria for optimizing the resonators, and to determine quantitatively the combinations of parameters which would yield the most beneficial effects of mode overlapping in both buncher and output resonators. The initial quantitative study of these parameter combinations was concerned mainly with resonators which would be suitable for use in the output stage of a broadband klystron. Detailed study of resonators for use in the buncher section will be carried out during the next period.

Also included in the investigation during this first period was a comparison of three different lumped-element circuits to represent the resonator. The purpose of the comparison was to determine which circuit was best from the standpoint of predicting the resonator interaction impedance as a function of frequency.

Details of the progress for this period are presented in the sections following.

TWO-GAP EXTENDED-INTERACTION RESONATORS WITH MODE OVERLAPPING

A. Introduction

It has long been the feeling among engineers involved with the design of broadband klystrons that the performance of this type of klystron could be improved through the use of extended-interaction resonators. This feeling is based on the advantages offered by these resonators, some of which are: (1) the resonator R_{sh}/Q can be higher than in a single-gap cavity; (2) the power density within an output resonator can be lower than that in a single-gap cavity by a factor of n^2, where n is the number of gaps; (3) an extended-interaction output resonator can produce a higher degree of electron bunching and therefore higher efficiency; and (4) it is possible to obtain lower values of beam-loaded Q in the extended-interaction resonator. The first three items above are important in the output stage of a klystron. The first and fourth items are advantageous in the buncher section.

The characteristics and theoretical performance of extended-interaction resonators in high-power broadband klystrons were studied extensively in a previous contract[1]. In that investigation, the extended-interaction resonators considered were restricted to single-mode resonators, wherein only one mode was excited at a time. It was shown that operation in the π mode is generally to be preferred in both the buncher and output sections at the megawatt-peak-power level chosen for the study. It was also shown that when the two resonator modes were separated sufficiently to assure single-mode operation, the π-mode R_{sh}/Q of a two-gap resonator was

substantially less than twice the R_{sh}/Q of the individual single-gap cavities. This was one of the primary factors influencing the results which led to the conclusion that single-gap cavities seem to be the best choice for the buncher section of high power broadband klystrons.

It was also observed that this latter conclusion might not hold if the modes were allowed to overlap in the extended-interaction buncher resonators. In this case, the resonators would be operated in more than one mode over the band, with the operation blending smoothly from one mode to another. By so doing, it seemed reasonable to expect that a higher interaction impedance over a greater bandwidth might be achieved in the individual resonators. Such a result would also be beneficial in an output resonator.

It is one of the primary goals of this contract to study extended-interaction resonators with mode overlapping. Much of the work during this first period was concerned with finding the interaction impedance of such resonators. The investigation initially is being restricted to resonators with two gaps. There are two reasons for this restriction. First, from the standpoint of both the theoretical analysis and the contemplation of future cold testing and construction of these resonators, it seems most reasonable to start with the simplest case. If it is deemed useful, the investigation can be extended to resonators with more gaps later. Second, by restricting the number of gaps to two, the possibilities of instability are minimized.

The analysis leading to the results reported in this section was based on the equivalent circuit described in Part B, below. The equations used in the analysis, and their derivation, are discussed in Appendix I.

Many of the calculations were performed with the aid of digital computers. Some guidelines for choosing the resonator parameters to be used in the computer calculations were obtained from an approximate analysis, in which the equations were simplified enough to be solved without the aid of a computer. Some help in the selection of parameters was also obtained from the thesis of Bert[2]. Most of the resonators studied during this first period had one cavity loaded to a low Q value, such as would be the case in a resonator to be used in the output stage of a broadband klystron.

B. Equivalent Circuit

The lumped-element equivalent circuit being used to represent two-gap extended-interaction resonators is shown in Fig. 1. The resistance shown in each cavity includes any external loading of that cavity as well as resistive losses in the cavity walls. The coupling between the two cavities is represented by a single element, the shunt inductance L_o. This circuit is very attractive both because of its simplicity and also because it simulates very well the general behavior of the two mode frequencies as a function of the coupling that exists in an actual inductively-coupled backward-wave resonator. In both this model and the actual resonator, the π-mode frequency decreases with increasing coupling while the 2π-mode frequency is practically unaffected. The value of the coupling inductance L_o can easily be related to the actual coupling in a cold test resonator from a knowledge of the frequencies of the two modes in the resonator before it is coupled to any external load. In the

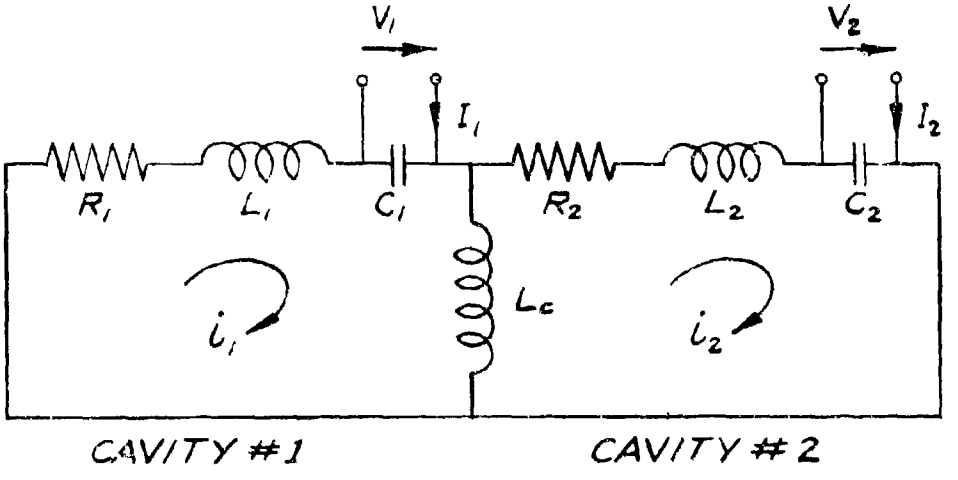

Fig. 1 - Inductively-coupled two-gap resonator equivalent circuit

lossless case with identical cavities,

$$\frac{f_{2\pi}}{f_{\pi}} = \sqrt{1 + 2\alpha} \tag{1}$$

where

$$\alpha = \frac{L_o}{L_1} \tag{2}$$

Two other lumped-element circuits, in which the coupling slots between cavities are represented by shunt resonant circuits, were also considered. They are discussed and compared with the circuit of Fig. 1 in the following section.

C. Modes of the Undriven Resonator

A great deal of insight into what happens in a resonator when the modes overlap can be gained by studying the properties of the modes in an undriven resonator (no rf excitation by the beam). As described in Appendix I, these modes may be found by solving for the complex frequency roots of Eq. (I-34):

$$|\underset{\sim}{K}| = 0 \tag{3}$$

where $|\underset{\sim}{K}|$ is the determinant of the circuit impedance matrix. The overall Q of the resonator in each mode may be found from these complex roots by use of the relation[3]

$$Q = \frac{\omega}{2\sigma} \tag{4}$$

where ω and σ are the real and imaginary parts of the complex frequency, respectively. The relative amplitudes and phase angles of the rf

gap voltages in each mode may be found by solving Eq. (I-37) at the complex frequencies of the modes.

A picture of the gap voltages at the modes of one resonator is shown in Fig. 2. Here the second cavity is loaded to a Q of 5, while the first cavity is unloaded. (Q_2 refers to the loaded Q of the second cavity before it is coupled to the first cavity.) The graph illustrates the change in V_2 relative to V_1 in the two modes when the coupling parameter α is varied. V_1 is arbitrarily chosen to be equal to $1 + j0$ in both modes. (It is convenient to choose V_1 for reference since the induced current in the first gap will be chosen for reference in the cases where the resonator is driven.)

It is seen that for large values of α the high frequency mode approaches a pure 2π mode (V_2 in phase with V_1) and the low frequency mode approaches a π mode (V_2 and V_1 π radians out of phase). As α decreases and the modes overlap more, both modes become distorted. However, the voltage vectors V_2 in the two modes do remain approximately symmetrically located with respect to the imaginary axis.

Figure 3 shows the gap voltage picture for this same resonator when the coupling is held constant at $\alpha = 0.1$, but the loading of the second cavity is changed. Here it is seen that the modes are nearly pure for high values of Q_2, but that they become more distorted as Q_2 is decreased.

These two figures indicate what one would intuitively expect to observe: that the degree of mode overlapping is a function of both the coupling between the cavities (frequency separation between the

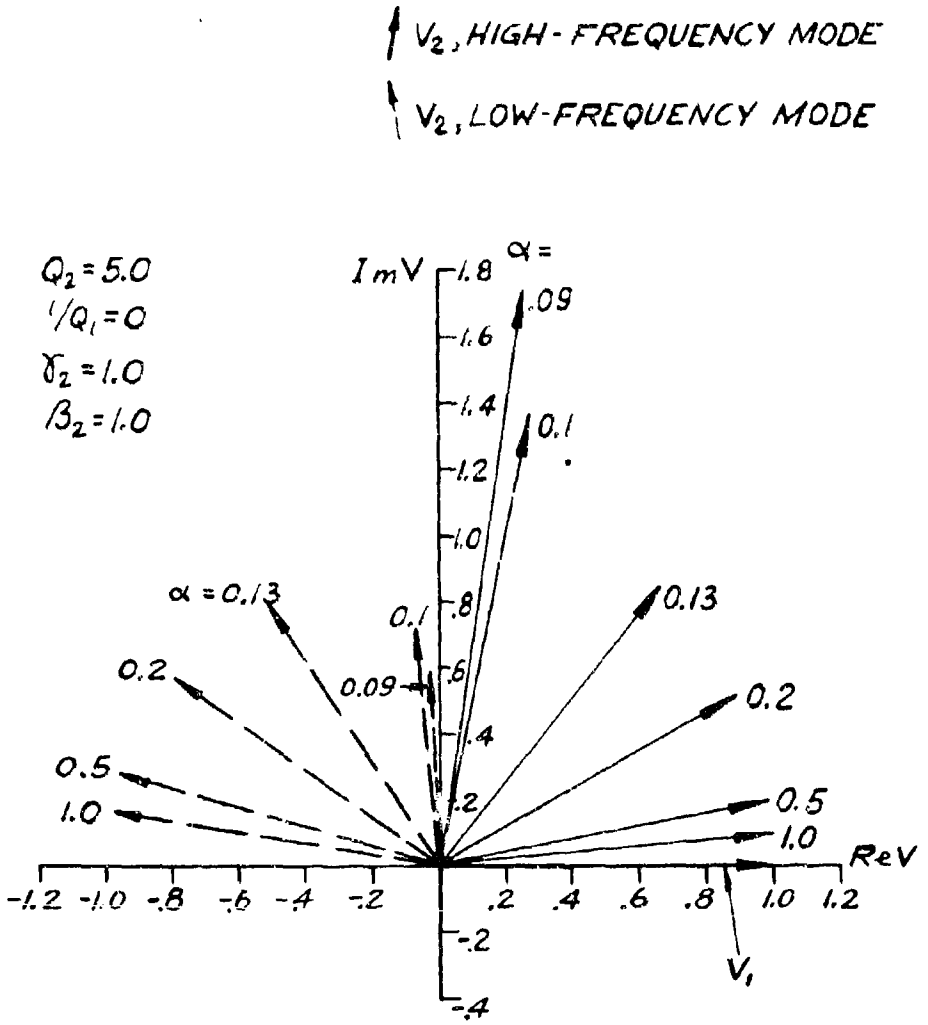

Fig. 2 - RF gap voltage vectors in a two-gap resonator as a function of the coupling parameter α. V_1 is used for a reference.

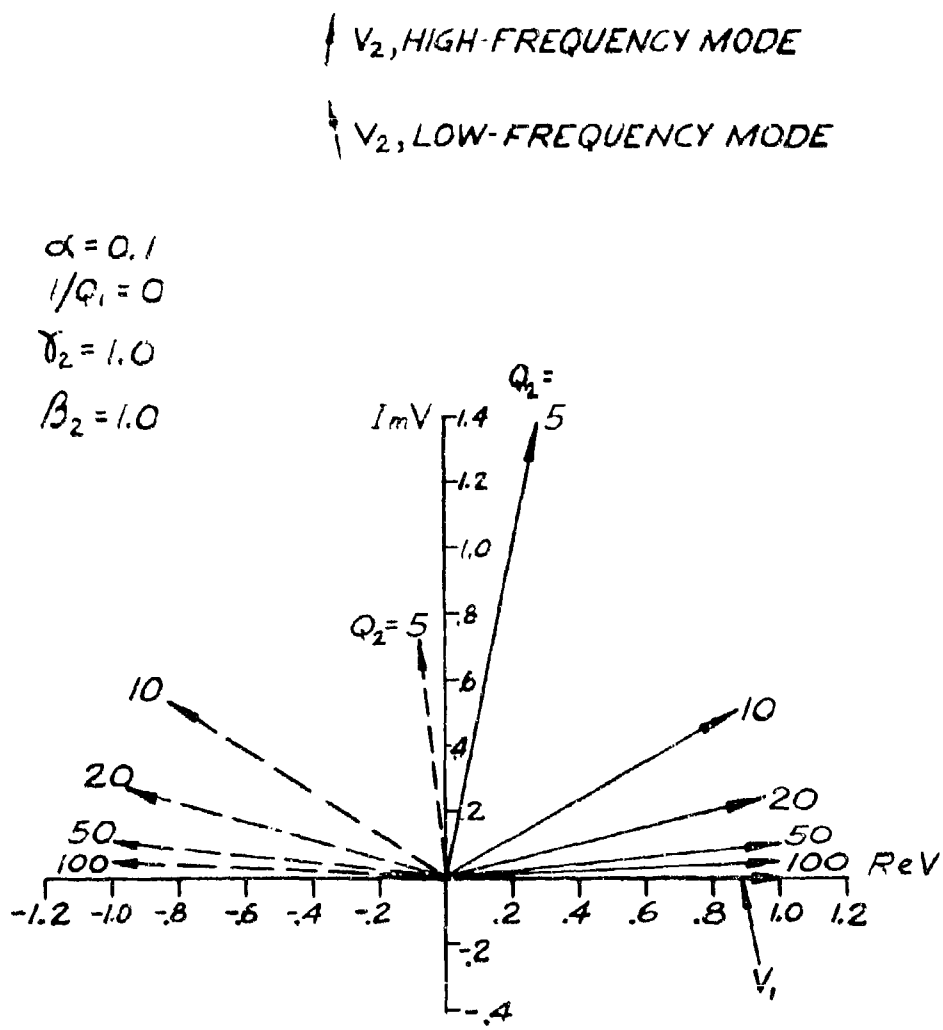

Fig. 3 - RF gap voltage vectors for a two-gap resonator as a function of the loaded Q of the second cavity.

two modes) and the loading of the resonator. For example, one would expect that for the modes to overlap in a high-Q resonator, they would have to be closely spaced in frequency. A detailed comparison of the voltage vectors in Figs. 2 and 3, taking into account the values of both the coupling parameter α and the Q of the loaded cavity in each case, even suggests that the degree of mode overlapping is determined by the product α Q. This is approximately true, but an examination of all of the elements of the interaction impedance expression shows that it is not exactly true.

The gap voltage diagrams in these two figures also give some information about the relative Q values of the overall resonator in the two modes. In this case, where the second cavity is loaded but the voltage on the first gap is used for reference, the mode with the lowest magnitude of V_2 will have the highest Q. (This can be seen by imagining what the picture would look like if V_2, the voltage in the loaded cavity, were used for reference, and by thinking of the definition of Q in terms of stored energy and power loss.) When the magnitude of V_2 is the same in both modes, the Q's of the two modes will be nearly equal when the frequency separation between them is small. (This will not be true for a large frequency difference between the modes because the loading of the second cavity varies with frequency.) It is seen that the Q's of the two modes are approximately equal when the amount of mode overlapping is moderate. However, for a large degree of overlapping the Q of one mode dominates, in this case the lower frequency mode.

In the resonator of Figs. 2 and 3, the capacitances and

inductances (and therefore also the unloaded resonant frequencies) of the two cavities were assumed to be equal. Figs. 4 and 5 show what happens to the gap voltages when the loaded cavity is detuned by changing its inductance (gap capacitances still equal). The ratio of the unloaded resonant frequencies of the two individual cavities is specified by the parameter $\gamma_2 = \omega_2/\omega_1$. The phase of V_2 in each of the two modes is changed only slightly, but the magnitude of V_2 is changed considerably. When the loaded cavity is tuned low, the Q of the low frequency mode decreases and the Q of the high frequency mode increases. The opposite is true if the loaded cavity is tuned high.

The mode frequencies and calculated Q's corresponding to the cases shown in Figs. 2-5 are listed in Table I.

D. Frequency Response of the Driven Resonator

The mode voltage diagrams presented above provide a good overall picture of what happens in the undriven resonator. However, they do not show what the continuous frequency response of the resonator will be when it is driven by a modulated beam. This response was found by calculating the power output from the resonator (power delivered to the load of the loaded cavity) as a function of frequency for specified rf drive currents. The interaction impedance of the resonator was also determined from this information. As described in Appendix I, the interaction impedance has been defined in terms of the output power and the rf drive current:

$$\mathrm{Re}\ Z_c = \frac{2P}{A^2} \qquad (5)$$

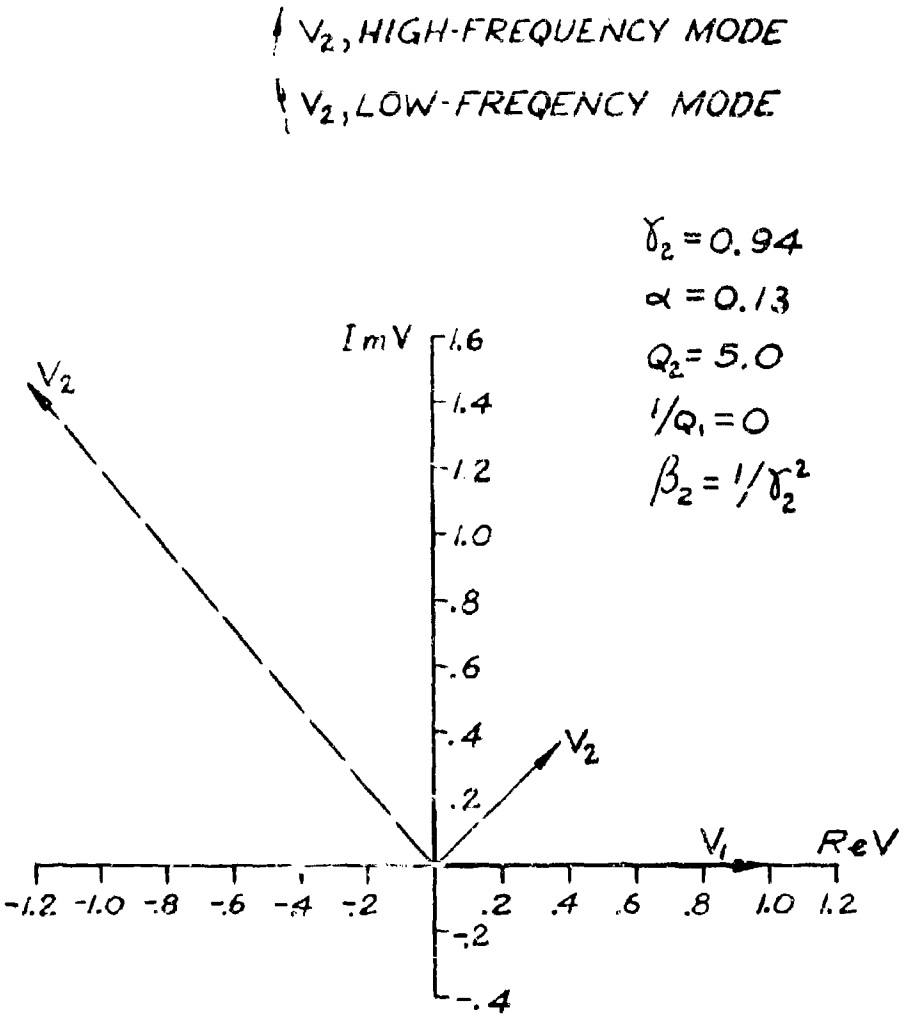

Fig. 4 - RF gap voltage vectors in a two-gap resonator. The loaded cavity is tuned low.

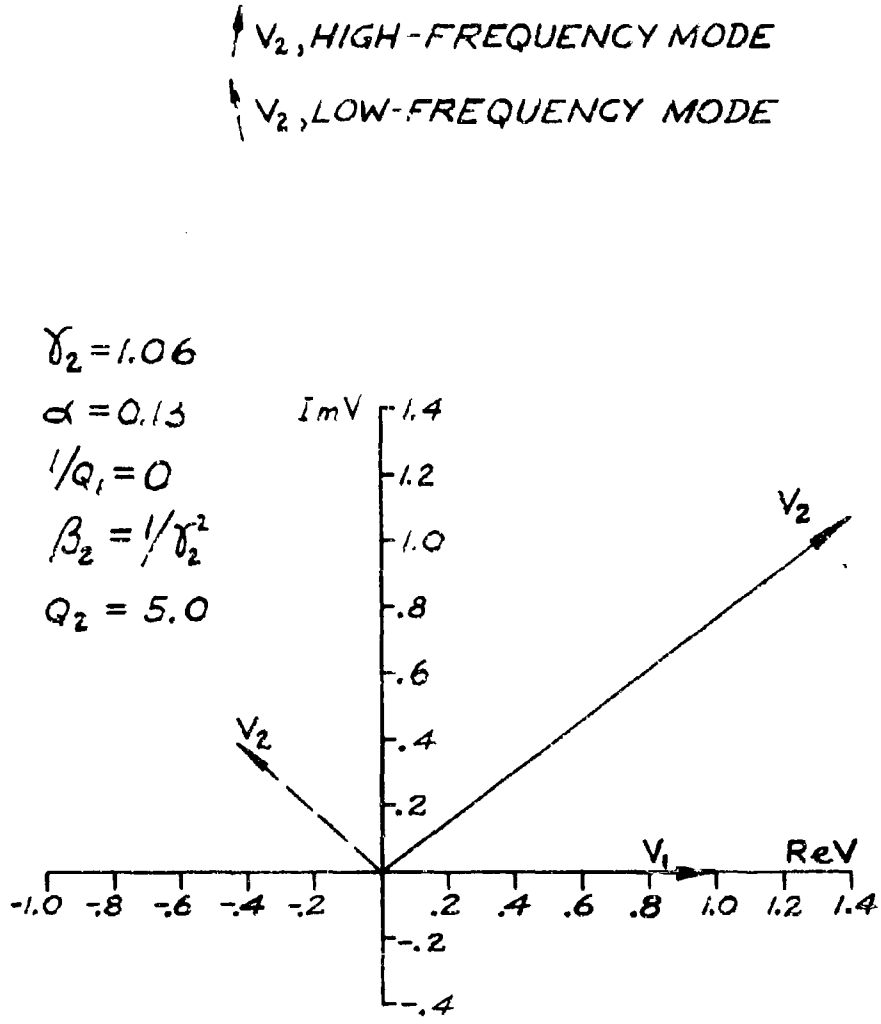

Fig. 5 - RF gap voltage vectors in a two-gap resonator. The loaded cavity is tuned high.

α	Q_2 at ω_1	γ_2	High Frequency Mode		Low Frequency Mode	
			Freq. ω/ω_1	Q	Freq. ω/ω_1	Q
0.09	5	1.0	.960	6.9	.956	21.4
0.1	5	1.0	.960	7.8	.949	15.6
0.13	5	1.0	.975	9.6	.912	11.7
0.2	5	1.0	.985	9.8	.856	12.0
0.5	5	1.0	.994	9.9	.710	14.2
1.0	5	1.0	.996	10.0	.579	17.3
0.1	10	1.0	.993	19.8	.919	22.1
0.1	20	1.0	.998	39.9	.914	43.9
0.1	50	1.0	1.000	100	.913	110
0.1	100	1.0	1.000	200	.913	219
0.13	5	.94	.961	22.5	.874	6.8
0.13	5	1.06	1.019	6.8	.918	23.7

TABLE I

Frequencies and Q's of the modes of the undriven resonator

where P is the power dissipated in the load, and A is the amplitude of the rf current induced in the first gap.

When specifying the rf excitation of the resonator, we have chosen to use the induced current in the first gap as a reference. So I_1 is given by

$$I_1 = A \tag{6}$$

where A is real. The most general expression for the current induced in the second gap is

$$I_2 = a_2 \, Ae^{j\theta_2} \tag{7}$$

The computer program which is used to calculate the power output from the resonator assumes that I_1 and I_2 occur simultaneously in time, whereas in an actual klystron the second gap is excited later in time than the first gap. The phase angle θ_2 is used to simulate the phase change of both the rf beam current and the gap voltages which takes place during the transit time of the beam between the first and second gaps in the actual situation. Since this transit time is normally small compared with one period of plasma oscillation, but is an appreciable fraction of the period of the rf drive frequency, the magnitude of θ_2 will be approximately equal to the normalized distance between the resonator gaps. In order to simulate a later time phase for I_2, θ_2 must be negative. Thus,

$$\theta_2 \approx - \beta_e p \tag{8}$$

where p is the spacing between the two gap centers and β_e is the

usual propagation factor associated with the dc beam velocity. It should be noted that at a constant beam voltage, θ_2 is a linear function of frequency. This has been taken into account in the calculations.

θ_2 will also be affected by changes in the average electron velocity due to the energy exchange between the beam and the resonator in the first gap. Changes in the amplitude of the rf beam current which accompany the modulation or demodulation of the beam in the first gap can be simulated by adjusting the coefficient a_2 to be greater than or less than unity. However, these effects of the beam modulation within the first gap were ignored initially in order to simplify the calculations and to obtain a general picture of the behavior of the driven resonator without having to specify particular beam and gap parameters.

The response of one resonator when driven by the beam is shown in Fig. 6, where the output power is plotted as a function of normalized frequency (normalized to the unloaded resonant frequency of the first cavity). Curves are shown for a number of different values of the coupling parameter α. The synchronization between the beam and the circuit (θ_2) has been fixed at a value that yields approximately equal output power in the two modes when $\alpha = 0.13$. The two cavities of the resonator are assumed to be equal, except that the second cavity has been loaded to a Q of 5 while the first cavity remains unloaded. The values listed for the current amplitude factor A and the R_{sh}/Q of the first cavity were chosen arbitrarily. The choice of these values does not affect the shape of the curves but only their

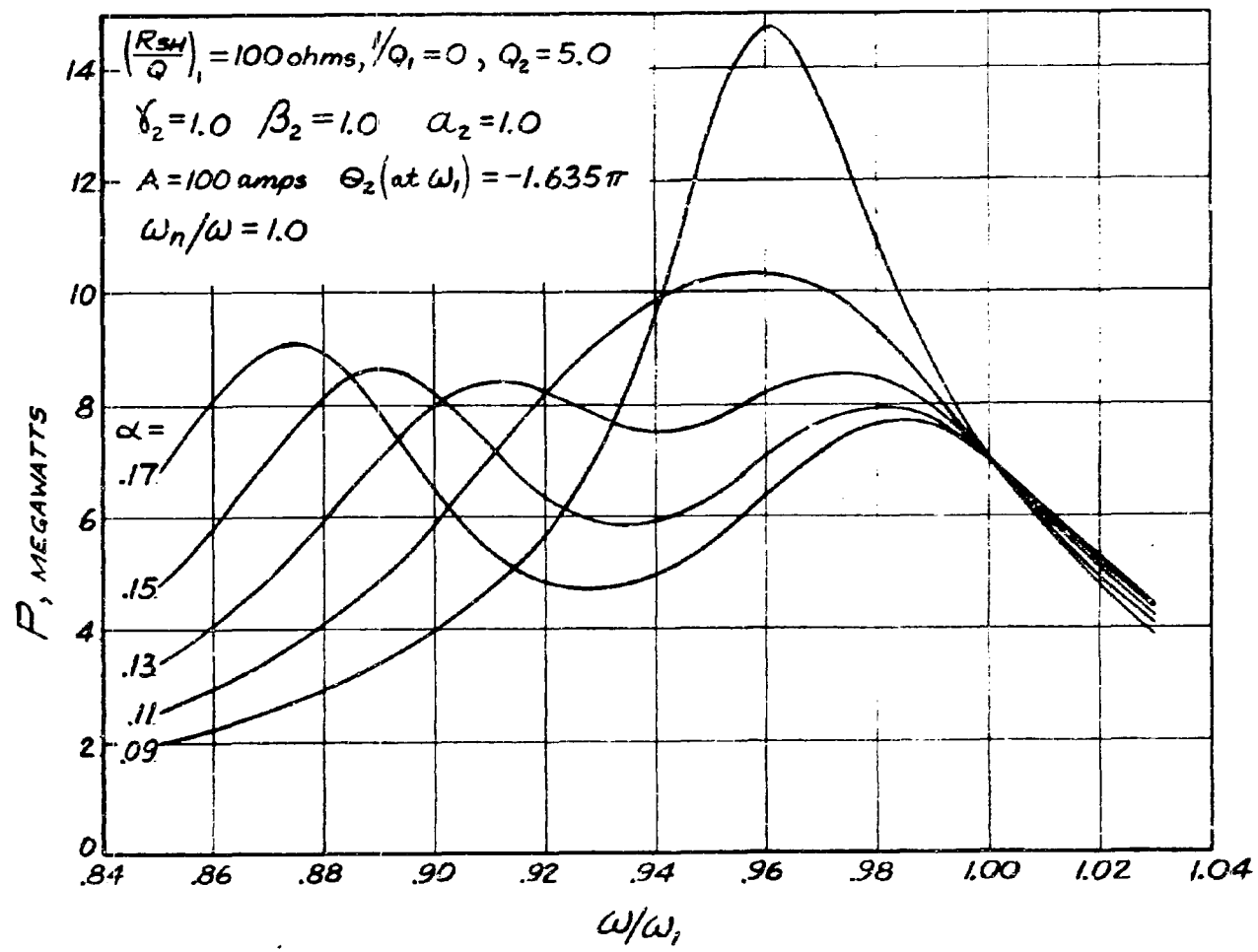

Fig. 6 - Power response of a two-gap driven resonator for different values of the coupling parameter α. The real part of the interaction impedance is proportional to the power.

amplitude (P is proportional to the product of $(R_{sh}/Q)_1$ and A^2).

The change in the response of the resonator as α is varied is consistent with what would be expected from a study of Fig. 2 and Table I. As α decreases, the frequency separation between the two modes also decreases. Furthermore, as α approaches the lowest value shown (.09) the two modes not only become very close in frequency, but the Q of the lower mode increases rapidly. Also, for the higher values of α in Fig. 6, one would expect that the beam should be synchronized approximately halfway between the two modes ($\theta_2 \approx -1.5\,\pi$), but that the higher frequency mode should be favored slightly since it has a slightly lower Q. This expectation is verified since in the case shown, $\theta_2 = -1.54\,\pi$ at the center of the resonator response ($\omega \approx .94\,\omega_1$).

The figure also illustrates how the bandwidth of the resonator changes as α varies. The 1 db bandwidth, for example, increases as α increases until the power output at the center of the response is 1 db below the peak power output. Beyond this, the power at the center of the response becomes a smaller fraction of the peak power and the 1 db bandwidth drops suddenly to a lower value. To take maximum advantage of the possible bandwidth increase, the beam synchronization should be adjusted until there is equal power output at the two modes.

The effect of synchronization changes on the response of this same resonator is shown in Fig. 7, where α and the other parameters are held constant while θ_2 is varied. It can be seen that the symmetry of the response is a fairly sensitive function of the beam synchronization.

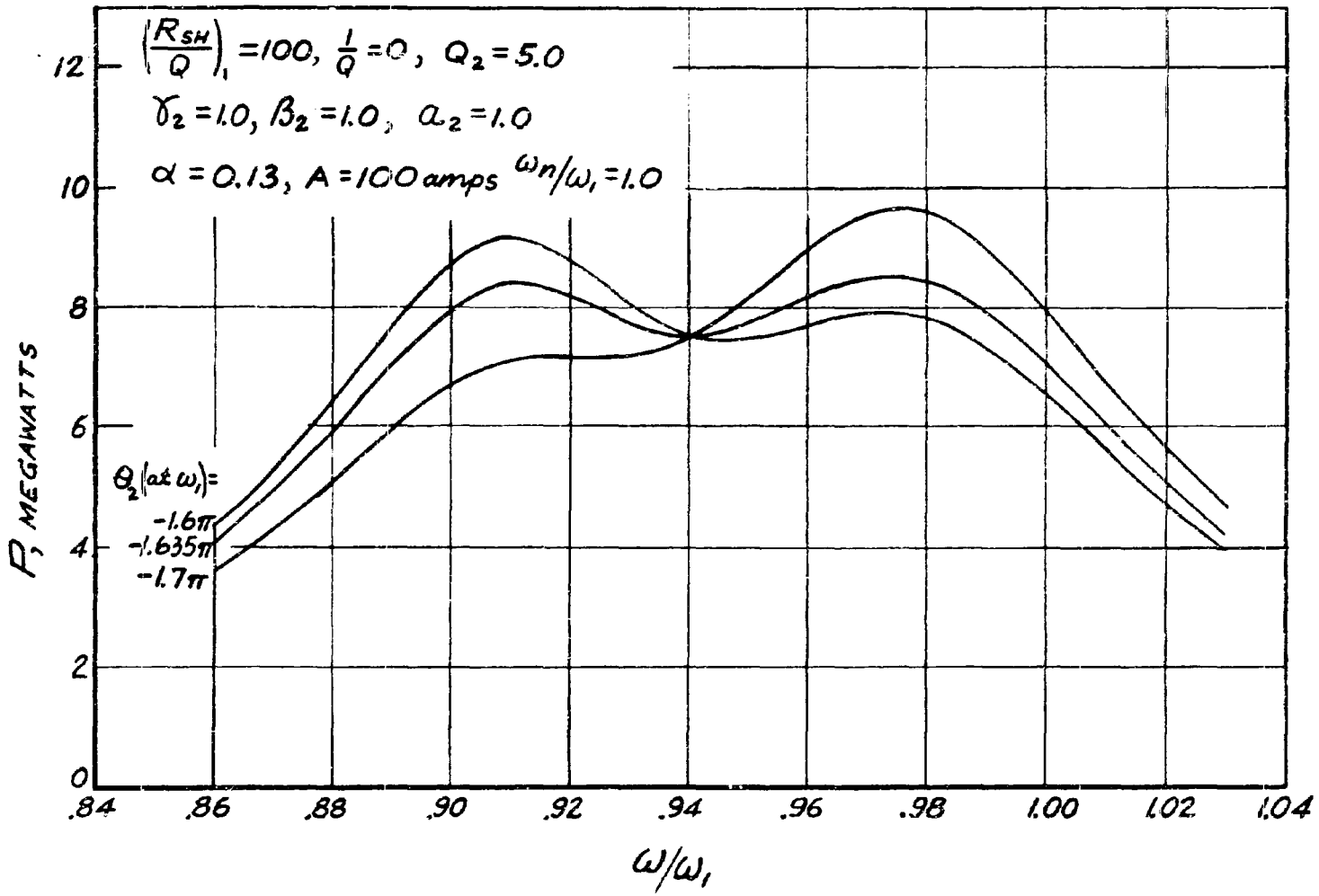

Fig. 7 - Power response of the two-gap driven resonator for three different values of the beam synchronization parameter.

It is informative to look at the gap voltage distribution in the driven resonator. The two gap voltages are plotted in Figs. 8, 9 and 10 at the frequencies of the two modes, and also at a frequency halfway between, for the case where $\alpha = 0.13$ and θ_2 (at ω_1) is $-1.635\ \pi$. In these plots I_1 (which is purely real) is used as a phase reference. The phase of I_2 is shown at each frequency. The amplitudes of I_1 and I_2 are equal and are presented in arbitrary units on these plots.

The two gap-voltage magnitudes are seen to be approximately equal at the three frequencies spanning the resonator response. This is important wherever uniformity of power dissipation within the resonator is of concern, as it would be if the resonator were to be used in the output stage of a high-average-power klystron. The figure also shows that the two gap voltages are approximately in phase with the respective induced gap currents. This indicates that there is power transfer from the beam to the resonator in both gaps.

It should be pointed out that the power response of the resonator (power output as a function of frequency) would be unchanged if the first cavity were loaded to the Q of five instead of the second cavity. However, the gap voltage distribution would be drastically altered. This is illustrated in Figs. 11, 12, and 13, where the gap voltages are plotted at the same three frequencies as in the previous three figures, but with the first cavity loaded. Here the magnitudes of V_1 and V_2 are quite unequal at all three frequencies. Furthermore, the phase of V_1 has changed considerably. V_1 is nearly 90° out of phase with I_1 near the two edges of the resonator response and is approximately 180° out of phase with I_1 at the center of the response. Thus

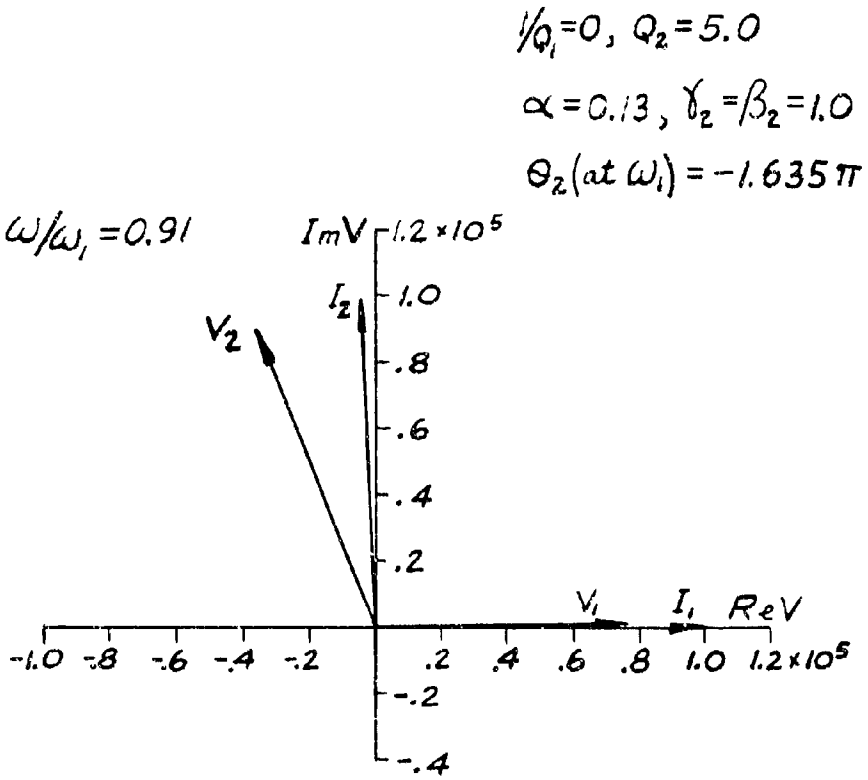

Fig. 8 - RF gap voltage and drive current vectors in the resonator of Fig. 6. $\alpha = 0.13$, $\omega/\omega_1 = 0.91$.

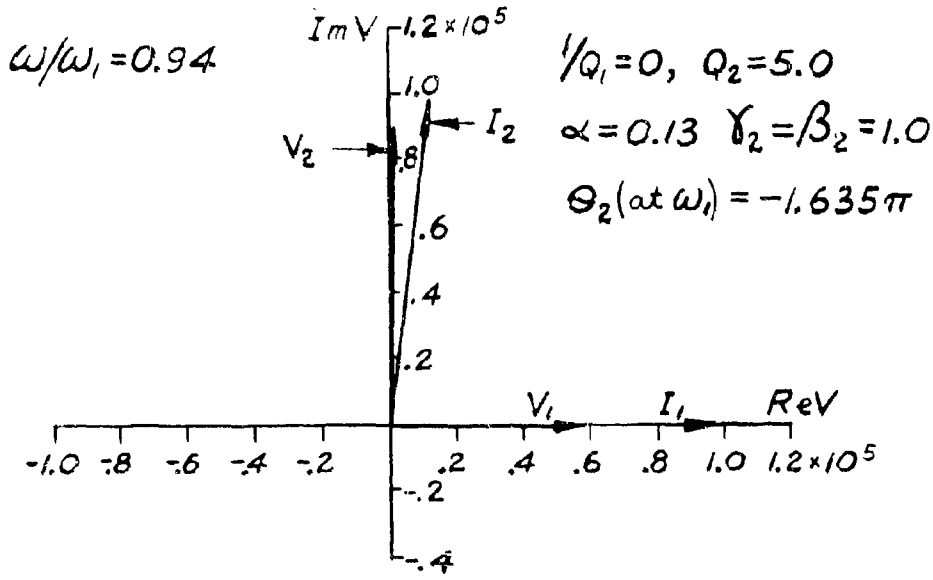

Fig. 9 - RF gap voltage and drive current vectors in the resonator of Fig. 6. $\alpha = 0.13$, $\omega/\omega_1 = 0.94$.

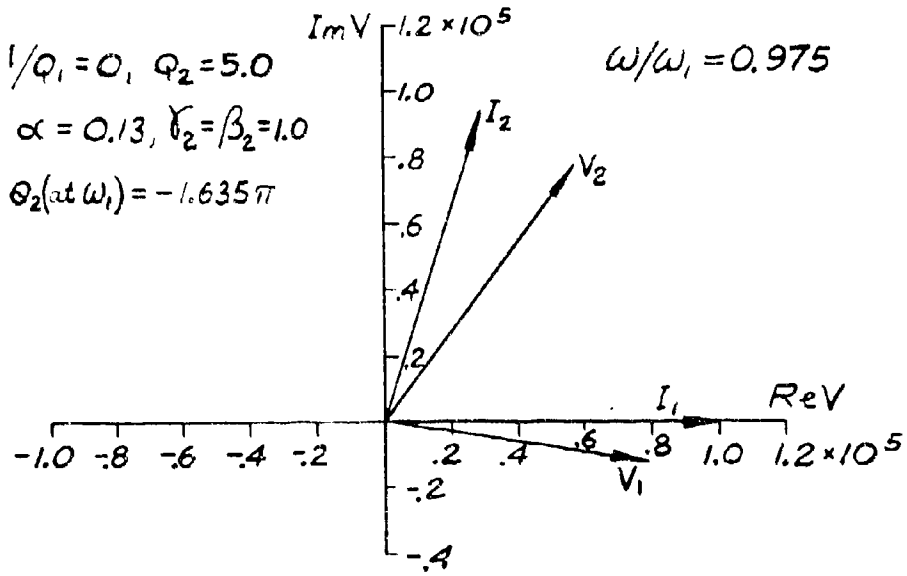

Fig. 10 - RF gap voltage and drive current vectors in the resonator of Fig. 6. $\alpha = 0.13$, $\omega/\omega_1 = 0.975$.

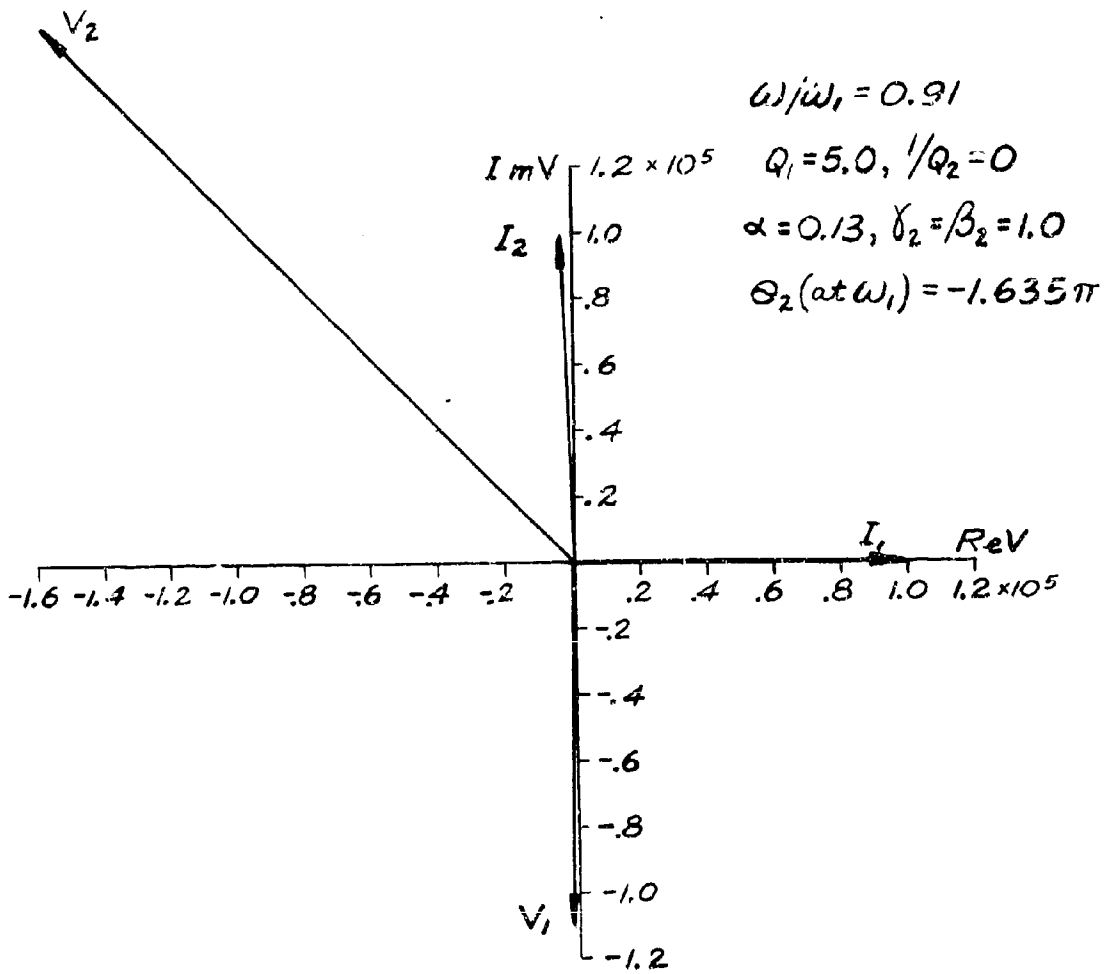

Fig. 11 - RF gap voltage and drive current vectors in the resonator of Fig. 6, except cavity #1 loaded. The power response is the same as shown in Fig. 6. $\alpha = 0.13$, ω/ω_1, = 0.91.

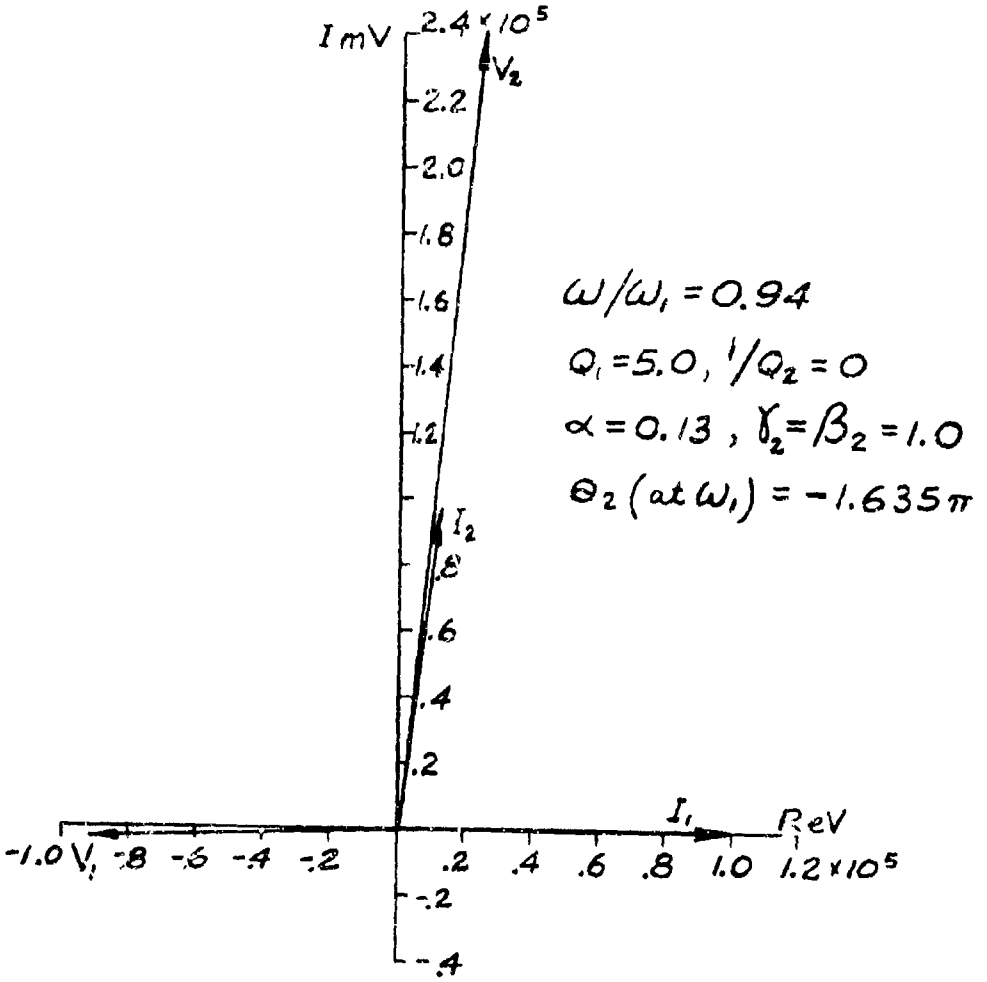

Fig. 12 - RF gap voltage and drive current vectors in the resonator of Fig. 6, except cavity #1 loaded. $\alpha = 0.13$, $\omega/\omega_1 = 0.94$.

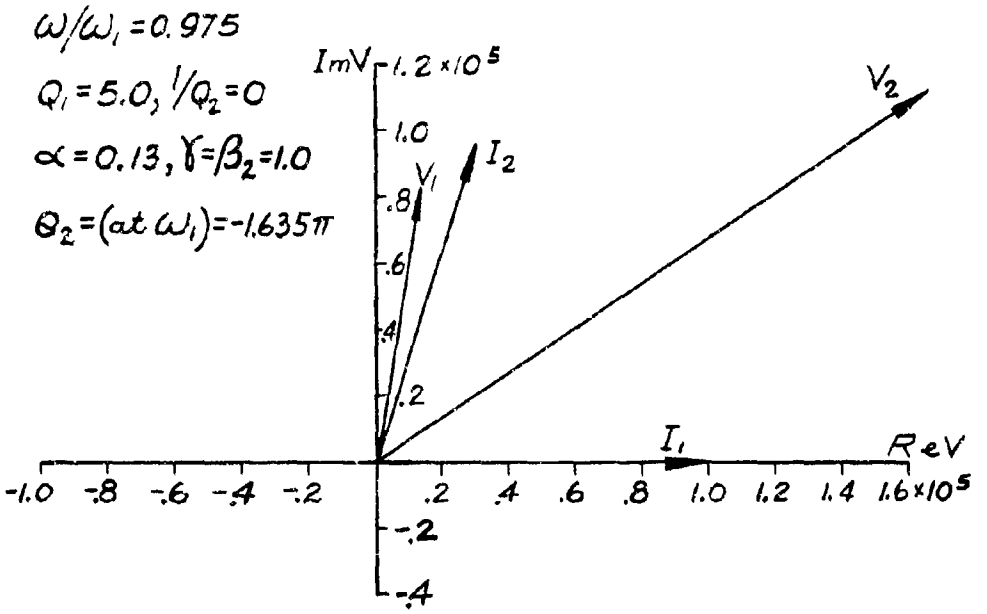

Fig. 13 - RF gap voltage and drive current vectors in the resonator of Fig. 6, except cavity #1 loaded. $\alpha = 0.13$, $\omega/\omega_1 = 0.975$.

there would be very little power transfer between the beam and the resonator in the first gap near the response edges, and a transfer of power from the resonator to the beam at the response center.

The relative voltage magnitudes and phase relationships between voltages and currents that exist in Figs. 8, 9, and 10 (cavity #2 loaded) can also be obtained when the first cavity is loaded if θ_2 is changed to approximately $-\pi/2$. However, in this instance the gap-to-gap spacing is so short ($\beta_e p \approx \pi/2$) that there would not be sufficient room for the wall between cavities in some cases.

When the loaded cavity of the resonator is detuned, the power response is affected as shown in Fig. 14. Here the second cavity is tuned low by increasing its inductance. The two gap capacitances are still assumed to be equal. The change in the Q's of the two modes is quite evident in this picture. In order to restore the condition of equal power output at the two modes, the beam synchronization must favor the mode with the lower Q (in this case, the lower frequency mode).

Figure 15 shows the resonator response for the case where $\omega_2/\omega_1 = 0.98$ and the synchronization has been properly adjusted. Figure 16 illustrates the response for the case where $\gamma_2 = 0.93$ and θ_2 at ω_1 is equal to -1.14π ($\theta_2 \approx -\pi$ at $\omega = .88\omega_1$). This latter case represents nearly the extreme of favoring the lower frequency mode (nominally the π mode). The gap voltage distribution corresponding to the response of Fig. 16 is shown in Figs. 17, 18, and 19.

A comparison of the 1 db bandwidths represented in Figs. 15, 16, and the $\gamma_2 = 1.0$ case of Fig. 14 shows that the bandwidth varies from

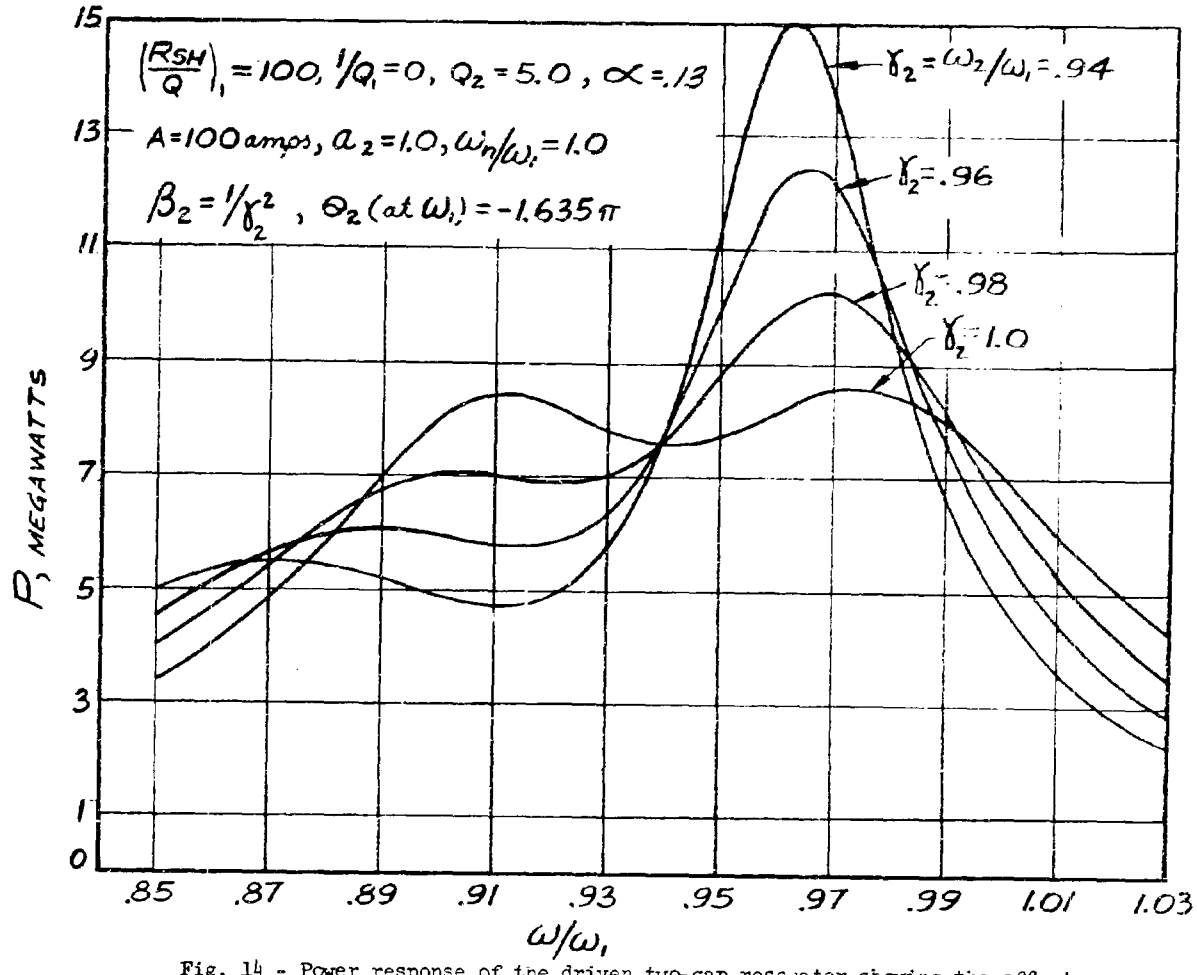

Fig. 14 - Power response of the driven two-gap resonator showing the effect of tuning the loaded cavity low while the other parameters are held constant.

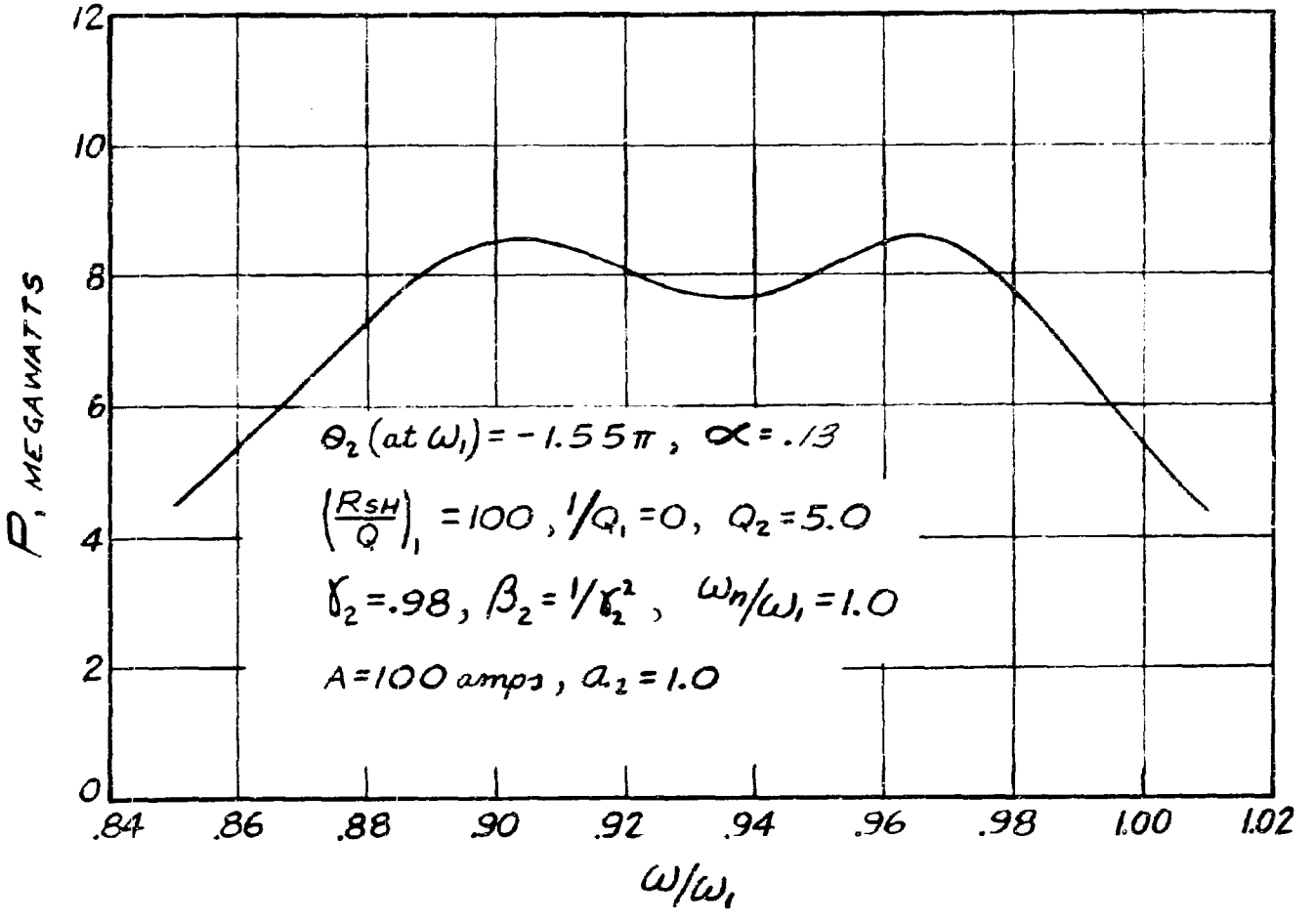

Fig. 15 - Power response of the two-gap driven resonator with the loaded cavity tuned low and the beam synchronization parameter adjusted for equal power output in the two modes. $\gamma_2 = 0.98$, $\theta_2(\text{at } \omega_1) = -1.55\pi$.

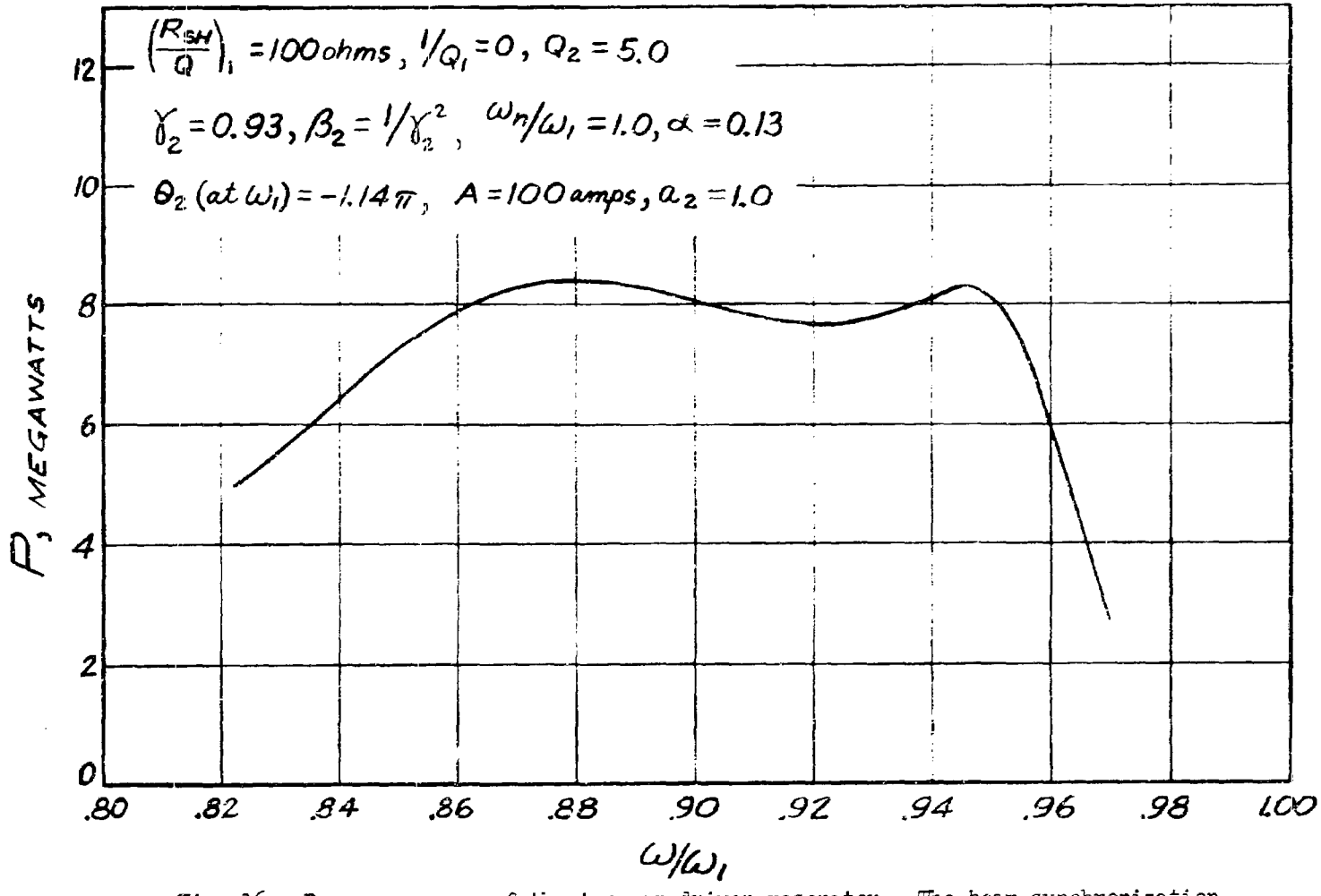

Fig. 16 - Power response of the two-gap driven resonator. The beam synchronization has been adjusted so $\varphi_0 = -\pi$ at the lower frequency mode, and the loaded cavity has been tuned low to yield equal power output in the two modes.

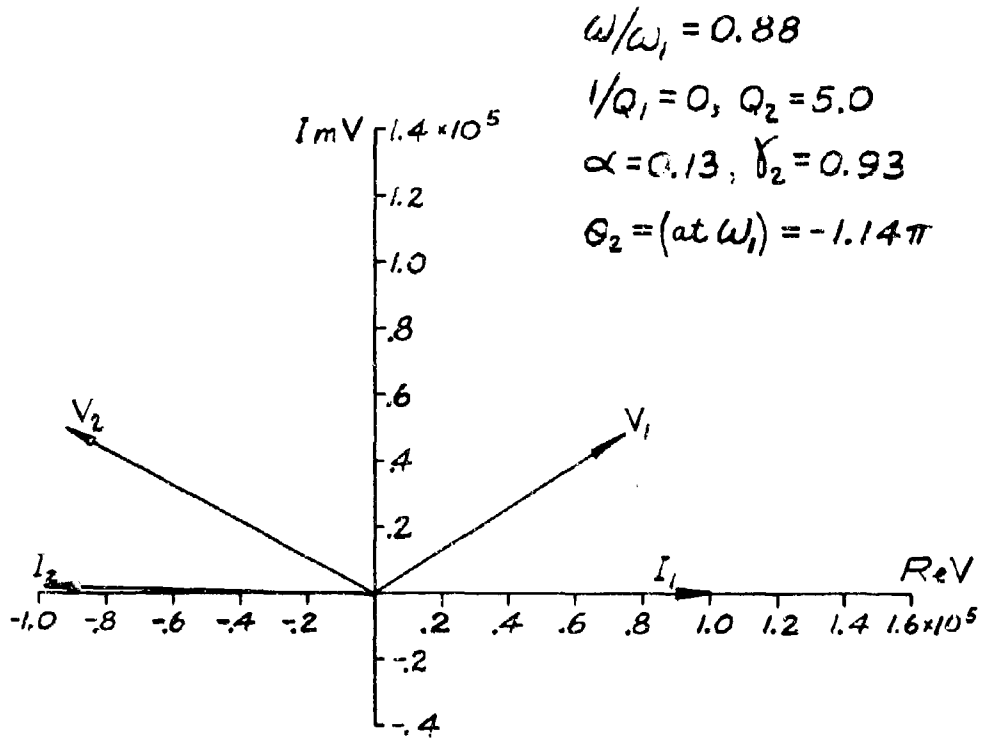

Fig. 17 - RF gap voltage and drive current vectors in the resonator of Fig. 16. $\omega/\omega_1 = 0.88$.

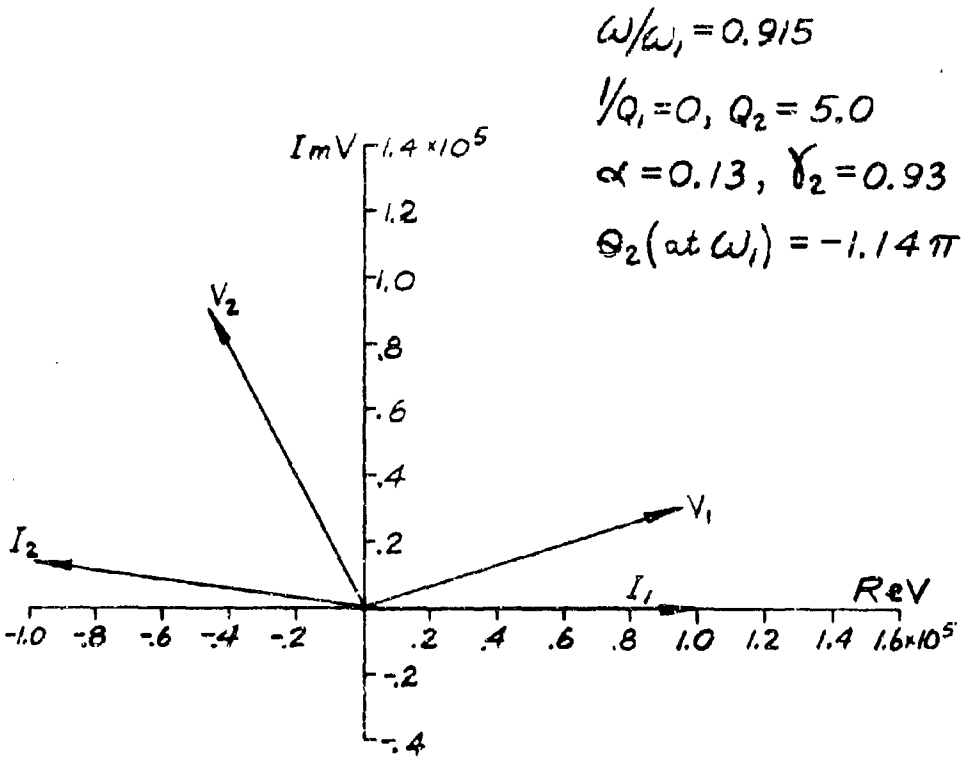

Fig. 18 - RF gap voltage and drive current vectors in the resonator of Fig. 16. $\omega/\omega_1 = 0.915$.

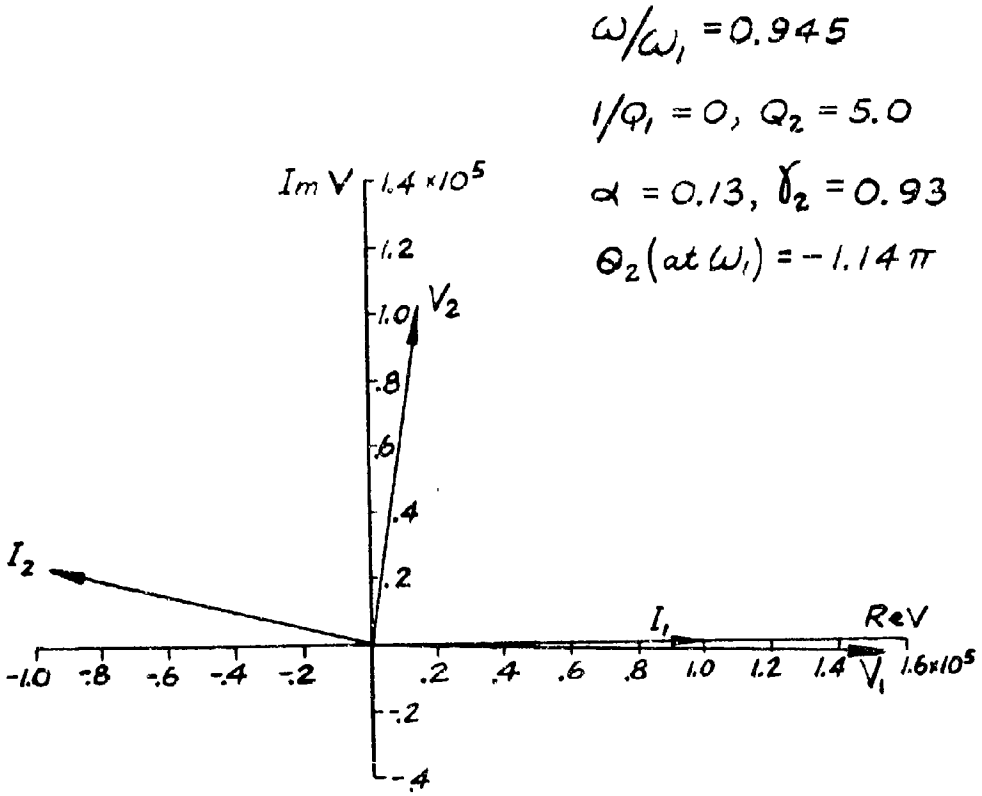

Fig. 19 - RF gap voltage and drive current vectors in the resonator of Fig. 16. $\omega/\omega_1 = 0.945$.

12.1 percent for $\gamma_2 = 1.0$ to 12.6 percent for $\gamma_2 = 0.93$. This indicates that there is no large bandwidth increase to be gained by detuning one of the cavities. However, the fact that the resonator can be shorter when the loaded cavity is tuned low ($\beta_e p \approx \pi$ in Fig. 16 while $\beta_e p \approx 1.6\ \pi$ in Fig. 14) might be advantageous. (The shorter resonator might have a more favorable cavity geometry and therefore a higher $(R_{sh}/Q)_1$ than the longer resonator.)

The information contained in Figs. 14, 15, and 16 points out the fact that the beam synchronization must be changed when one cavity is detuned. However, this also suggests the possibility of compensating for the change in the beam synchronization which accompanies a change in the operating beam voltage by tuning one of the resonator cavities.

It is realized that the 12 percent 1 db bandwidth predicted in the figures presented above does not meet the 14 percent objective of this contract. However, the purpose of presenting these curves is to show the general behavior of the resonator with changes in the parameters, and not necessarily what is required to achieve the full 14 percent bandwidth. A comparison of the mode overlapping resonator with other resonator types is presented below.

E. Bandwidth Comparisons Between Different Resonator Types

It was demonstrated above that the bandwidth of a two-gap resonator can be increased by employing mode overlapping and properly choosing the resonator and beam parameters. But in order to fairly evaluate the merits of any particular type of resonator, its bandwidth capabilities must be compared with other resonator types at a constant impedance level.

The impedance and bandwidth of single-mode resonators can be deduced from the values of Q and R_{sh}/Q measured at the mode of interest. At the resonant frequency of the mode, the impedance, both real and at a maximum, is given by

$$(\mathrm{Re}\ Z)_{max} = \left(\frac{R_{sh}}{Q}\right) Q \tag{9}$$

Let the 3 db bandwidth of the resonator be defined in terms of the frequencies at which the real part of the impedance is one half the maximum value (total impedance magnitude down by a factor of $1/\sqrt{2}$). Similarly, let the 1 db bandwidth be defined in terms of the frequencies at which the real part of the impedance is 80 percent of the maximum value. The 3 db and 1 db bandwidths are then related to the Q by

$$\left(\frac{\Delta f}{f}\right)_{3\ db} = \frac{1}{Q} \tag{10}$$

and

$$\left(\frac{\Delta f}{f}\right)_{1\ db} = \frac{1}{2Q} \tag{11}$$

In resonators where the modes are not distinctly separated, such as in filter-loaded resonators or extended-interaction resonators operating with mode overlapping, the concepts of R_{sh}/Q and Q are not directly applicable. In these cases, the interaction impedance is best determined by direct measurement. However, at the time of the writing of this report, no cold tests had been performed on mode-overlapping resonators similar to the ones being reported on theoretically. Therefore for the purposes of the comparison being made in this

section, the impedance as predicted by the equivalent circuit will be used.

It should be noted that there is some ambiguity involved in the use of the circuit of Fig. 1 when predicting the impedance of resonators with overlapping modes. The ambiguity arises in connection with the fact that this circuit predicts a higher R_{sh}/Q for the π mode than for the 2π mode when the gap capacitance is assumed to be independent of frequency. This is contrary to experimental observation in an inductively-coupled backward-wave resonator. However, no serious problem is raised when using this circuit in the analysis of single-mode resonators, where the modes are separate and distinct. In this case the circuit capacitance can be defined in terms of the experimentally measured frequency and R_{sh}/Q of the mode of interest (see Eq. I-23). But when trying to predict the interaction impedance of a resonator with mode overlapping, it was not immediately clear which mode to use to define the equivalent gap capacitance. If the capacitance is defined in terms of the π-mode R_{sh}/Q, the predicted impedance over the entire resonator bandwidth will be less than if the capacitance value is based on the 2π-mode R_{sh}/Q, even though the operation of the resonator includes both modes, blending smoothly from one to the other.

Because of this uncertainty, other equivalent circuits were studied in an effort to find one which would fairly accurately predict the experimentally observed change in the π-mode R_{sh}/Q as a function of the mode separation. Two circuits were considered in detail. A discussion of these circuits and a comparison of them with

the circuit of Fig. 1 are presented in the following section. The conclusion reached there is that the circuit of Fig. 1 should be used, and that the gap capacitance values should be defined in terms of the R_{sh}/Q and resonant frequency of the individual cavities (the two cavities before they are loaded or coupled to each other). This is what was done in the calculations of the response curves presented in this section.

For an example case of a resonator with mode overlapping, choose the curve with $\gamma_2 = 1.0$ in Fig. 14. (It should be noted that the power is down only 0.5 db at the center of the response, so this case represents less than the maximum 1 db bandwidth available for $Q_2 = 5$.) The value assumed for $(R_{sh}/Q)_1$ was 100 whereas previous cold-test measurements have shown that a value of 110 is reasonable to assume for a single-gap cavity.[4] Taking this into account (P is proportional to $R_{sh}/Q)_1$ in Fig. 14) and calculating the real part of the interaction impedance from Eq. (5), we find that the maximum value of Re Z_c is approximately 1850 ohms.

Using this value of impedance as a reference, Table II shows a comparison between the 1 db and 3 db bandwidths of three different types of resonators. The values of R_{sh}/Q assumed for the two single-mode resonators were based on previous cold test measurements[4,5]. The values of Q shown were calculated using Eq. (9).

Even allowing for some error in the predicted impedance level, it is seen that the use of mode overlapping in the two-gap resonator offers a substantial increase in the resonator bandwidth at a given impedance level. The bandwidth advantage over the two-gap single-mode

Resonator Type	R_{sh}/Q ohms	$(\mathrm{Re}\ Z_c)_{max}$ ohms	Q	Bandwidth	
				1 db	3 db
Two-gap with mode overlapping	$(R_{sh}/Q)_1 = 110$	1850	---	12.1%	17.6%
Two-gap, π mode (single-mode)	$(R_{sh}/Q)_\pi = 140$	1850	13.2	3.8%	7.6%
Single-gap	$R_{sh}/Q = 110$	1850	16.8	3.0%	5.0%

TABLE II

Comparison of the bandwidths of different types of resonators at a constant impedance level

resonator is approximately three to one, and close to four to one over the single-gap cavity. These bandwidth advantage figures are consistent with those predicted by Bert.[2]

There is one other type of resonator that should be compared with the mode-overlapping resonator, and that is the filter-loaded resonator. We have no data presently available on the two types of resonators where they are designed for equal bandwidth. However, the maximum value of Re Z_c predicted for one filter-loaded two-gap resonator with a 15 percent 1 db bandwidth was approximately 1300 ohms.[6] Thus the impedance level of this type of resonator is comparable to that of the two-gap resonator with mode overlapping. If it is assumed that the maximum impedance is inversely proportional to the bandwidth, the mode-overlapping resonator would have a slightly higher impedance at a given bandwidth.

INVESTIGATION OF TWO ADDITIONAL EQUIVALENT CIRCUITS TO REPRESENT COUPLED - CAVITY RESONATORS

A. Introduction

The equivalent circuit chosen to represent two-gap extended-interaction resonators for the analysis presented in the preceding section was shown in Fig. 1. This circuit was described briefly in the previous section. It was pointed out that the circuit simulated very well the general behavior of the two resonator mode frequencies as a function of the coupling between the two cavities. It was also mentioned that the circuit did not properly predict the π-mode R_{sh}/Q of the resonator. In fact, the predicted π-mode R_{sh}/Q is higher than the 2π-mode R_{sh}/Q (when the gap capacitances are assumed to be independent of frequency) whereas the opposite is true in the experimental case. This led to an uncertainty in how to choose the equivalent gap capacitances when using the circuit to predict the interaction impedance of resonators with overlapping modes. We therefore felt that a different equivalent circuit should be used, one which would quite accurately predict not only the resonator modes, but also the R_{sh}/Q of the resonator in the two modes.

The principal reason why the π-mode R_{sh}/Q is lower than the 2π-mode R_{sh}/Q in an inductively-coupled multiple-cavity resonator is that a portion of the electromagnetic energy in the resonator is stored in the slots at the π mode. Of this energy, the electric energy (energy in the electric field) is of primary interest in a klystron resonator since the beam is modulated by the axial component

of the electric field. The R_{sh}/Q is therefore normally defined in terms of the rf gap voltage and electric stored energy. The equivalent circuit of Fig. 1 does not simulate the lowered π-mode R_{sh}/Q because the coupling inductance L_o does not store any energy in electric fields. The search for a more adequate equivalent circuit was therefore directed towards circuits in which the coupling circuit does store electric energy and also retains its inductive nature.

Two circuits were investigated in detail. The circuit equations of both were solved for the frequencies of the characteristic modes in the cases where the two resonator cavities were assumed to be identical and lossless. Expressions were also derived for the R_{sh}/Q of the circuits at the two modes of the main passband. Theoretical values of the π-mode R_{sh}/Q were then compared with cold-test results. The cold-test resonators used for the comparisons were high-Q resonators, which closely approximated the lossless condition assumed in the theoretical calculations.

B. First Equivalent Circuit

The simplest modification that can be made to the circuit of Fig. 1 in order to simulate the electric energy storage in the coupling slots of an actual resonator is shown in Fig. 20. The coupling circuit has been made resonant by adding a capacitor in parallel with the coupling inductance. (A series resonant circuit could also have been used, but the parallel circuit better represents the actual coupling slots.) The capacitor stores electric energy while the coupling circuit still appears inductive as long as its

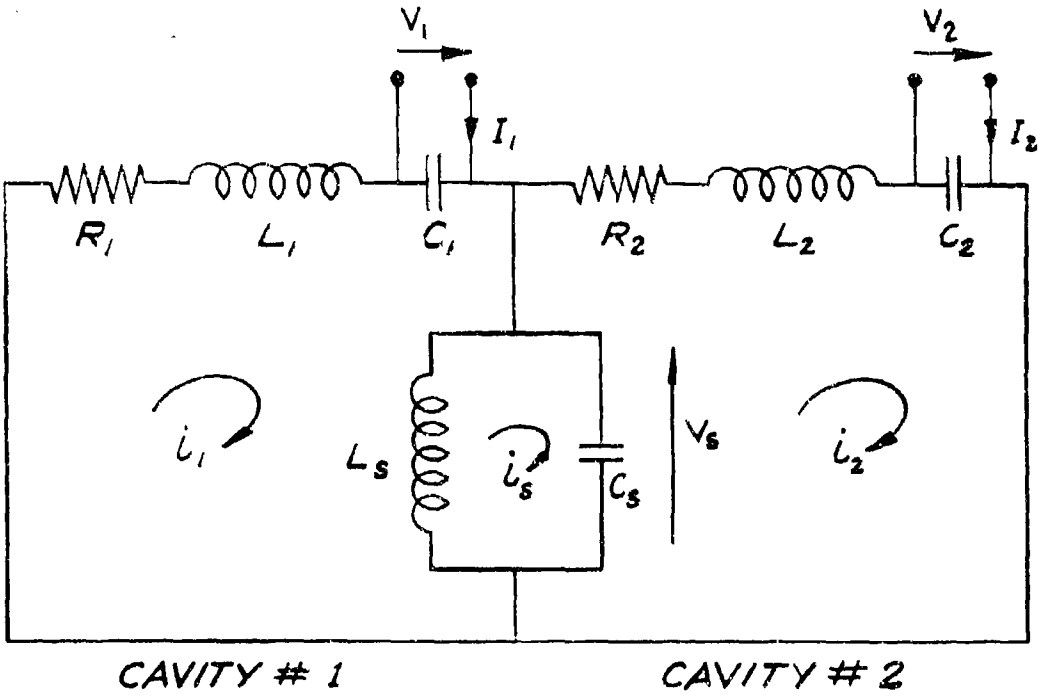

Fig. 20 - Two-gap resonator equivalent circuit with resonant coupling.

resonant frequency is higher than the operating frequency. This equivalent circuit is essentially the same as the circuits used by Chodorow[7] and Allen[8] to represent slot-coupled structures.

1. Modes of the Lossless Circuit

The modes of the circuit of Fig. 20 were found for the particular case where the two resonator cavities are assumed to be identical and lossless. This was done by setting $L_1 = L_2$, $C_1 = C_2$, $R_1 = R_2 = 0$, and applying Kirchhoff's laws to the circuit. The resulting equations were then solved for the frequencies at which the circulating currents i_1, i_2, and i_s are non zero when the two induced currents I_1 and I_2 are zero. This process yields three modes. At one of these modes, the currents i_1 and i_2 are equal in both magnitude and phase. Its frequency is

$$\omega_a = \frac{1}{\sqrt{L_1 C_1}} = \omega_1 \tag{12}$$

where ω_1 is the resonant frequency of the lossless and uncoupled first cavity of the resonator.

At the other two modes of the circuit, i_1 and i_2 are equal in magnitude but 180 degrees out of phase. One of these modes is at the frequency given by

$$\frac{\omega_b}{\omega_1} = \left[\frac{2}{1 + 2\frac{L_s}{L_1} + \left(\frac{\omega_1}{\omega_s}\right)^2 + \sqrt{\left[1 + 2\frac{L_s}{L_1} + \left(\frac{\omega_1}{\omega_s}\right)^2\right]^2 - 4\left(\frac{\omega_1}{\omega_s}\right)^2}} \right]^{1/2} \tag{13}$$

The frequency of the third mode, which could be denoted by ω_c, can be found from Eq. (13) by replacing the plus sign in front of the radical in the denominator by a minus sign. Note that ω_b is less than ω_1 and ω_c is greater than ω_1.

The two-gap cold-test resonators chosen for the comparisons with this circuit were similar to the resonator depicted in Fig. 21. The observed 2π-mode frequencies were all approximately the same as the frequency of the uncoupled cavities of the resonator, which agrees closely with the 2π-mode frequency given by Eq. (12). The measured operating π-mode frequency of each resonator was less than the 2π-mode frequency. Thus the frequency ω_b corresponds to the observed π-mode frequency.

2. R_{sh}/Q of the Circuit

There are a number of different ways to define both the Q and the shunt resistance of a circuit such as the one in Fig. 20. We have chosen to use definitions in terms of stored energy, power loss, and effective voltage. Using these definitions, the general expression for R_{sh}/Q can be written[9]

$$\frac{R_{sh}}{Q} = \frac{V^2}{2\omega U} \tag{14}$$

We have defined the effective voltage V of the circuit to be

$$V = \left|V_1\right| + \left|V_2\right| \tag{15}$$

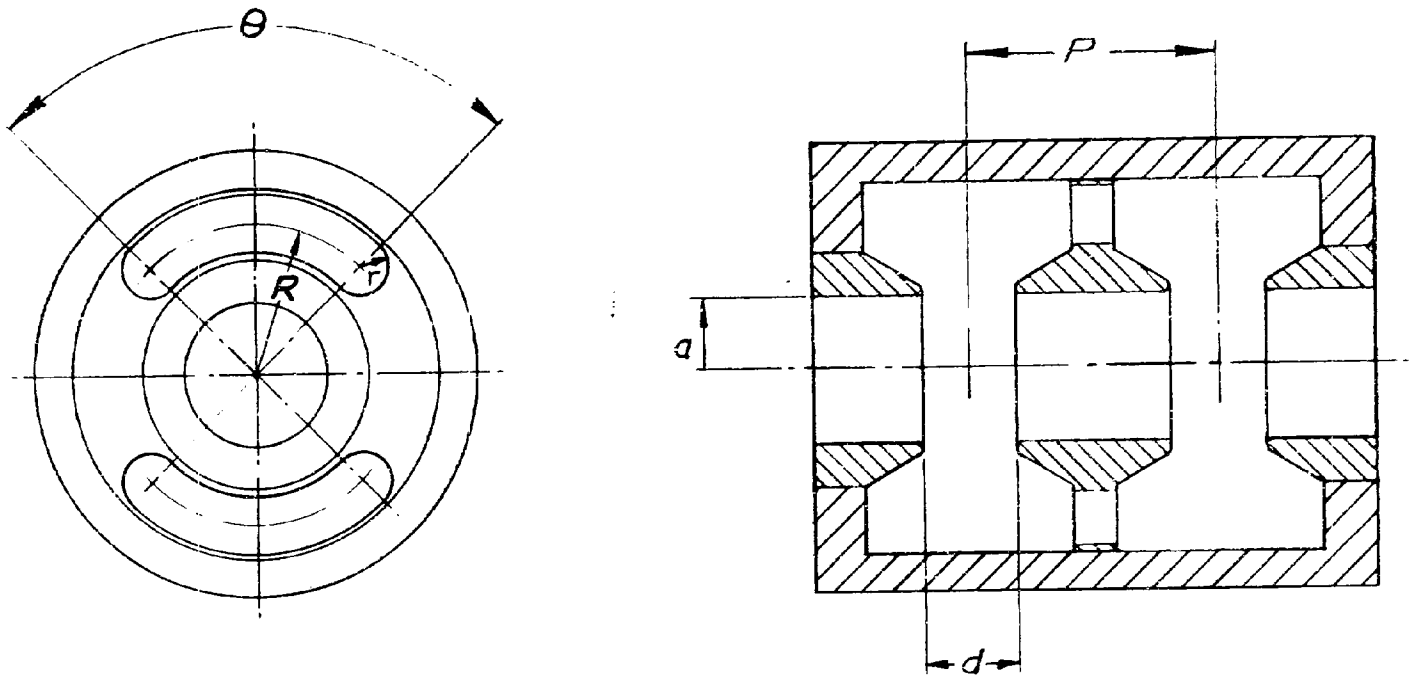

Fig. 21 - Typical two-gap extended-interaction resonator.

The electric stored energy is given by

$$U = \frac{1}{2}\left(C_1 V_1^2 + C_2 V_2^2 + C_s V_s^2\right) \tag{16}$$

Using Eqs. (14), (15), and (16), the R_{sh}/Q of the circuit of Fig. 20 (with lossless, identical cavities) was evaluated at the two frequencies $\omega_a = \omega_{2\pi}$ and $\omega_b = \omega_\pi$. The results are

$$\left(\frac{R_{sh}}{Q}\right)_{2\pi} = 2\left(\frac{R_{sh}}{Q}\right)_1 \tag{17}$$

$$\left(\frac{R_{sh}}{Q}\right)_{\pi} = \frac{2\left(R_{sh}/Q\right)_1}{\frac{\omega_\pi}{\omega_1}\left[1 + \frac{2\left(\frac{\omega_\pi}{\omega_1}\right)^2 \frac{L_s}{L_1}}{\left(\frac{\omega_s}{\omega_\pi}\right)^2\left[1 - \left(\frac{\omega_\pi}{\omega_s}\right)^2\right]^2}\right]} \tag{18}$$

where $(R_{sh}/Q)_1$ is the R_{sh}/Q of the uncoupled first cavity. It is related to the resonant frequency and capacitance of this cavity by

$$\left(\frac{R_{sh}}{Q}\right)_1 = \frac{1}{\omega_1 C_1} \tag{19}$$

Note that Eq. (19) is consistent with Eq. (14).

3. Comparison with Experimental Cases

When comparing the predictions of an equivalent circuit with measured values from a physical resonator, it is necessary

to correctly choose the circuit parameters to properly simulate the real case. The values of the cavity inductance and capacitance to use (e.g., L_1 and C_1) can be determined from measurements of the resonant frequency and R_{sh}/Q of the uncoupled cavity by using Eqs. (12) and (19). The value of cavity resistance to use (e.g., R_1) for a lossy or loaded cavity can be determined from the measured Q of the cavity. When using the circuit of Fig. 1, the value of L_c to use for the coupled-cavity resonator can be found from measured values of the frequencies of the two modes in the resonator before it is coupled to any external load (see Eq. (1)). When using the circuit of Fig. 20, two parameters are required to completely specify the degree of coupling between the two cavities. We have chosen these parameters to be the slot resonant frequency ω_s and the slot inductance L_s. It is convenient to normalize these parameters to the frequency and inductance of the uncoupled first cavity. Thus the actual coupling parameters used in the calculations were ω_s/ω_1 and L_s/L_1. The criteria used for the selection of the numerical values of these parameters assumed in the calculations are described below.

The resonant frequency of a coupling slot is related to the slot dimensions. In the case of a long, narrow slot, the resonant frequency will be quite close to the frequency at which the slot is one-half wavelength long. In terms of the dimensions shown in Fig. 21,

$$f_s \approx \frac{c}{2\,(R\theta + 2r)} \tag{20}$$

where c is the velocity of light expressed in the same units of length as R and r, and θ is given in radians. If R and r are given in inches and θ in degrees, Eq. (20) can be rewritten:

$$f_s \approx \frac{5.905}{R\left(\frac{\theta}{57.3}\right) + 2r}\ \text{GHz} \tag{21}$$

Scott and Wanselow[10] have found that Eqs. (20) and (21) predict a frequency which is too low when the slot width (2r) is not small compared to the slot length. They have reported an empirical formula for finding the frequency of slots like the ones shown in Fig. 21 when they are used in structures similar to the one shown in the figure. Their formula is

$$f_s \approx \frac{5.905}{R\left(\frac{\theta}{57.3}\right) + \sigma r}\sqrt{1 + \left(\frac{\theta}{180}\right)^2}\ \text{GHz} \tag{22}$$

where R and r are specified in inches, and θ is given in degrees. The coefficient σ is a function of the 2π-mode frequency, or very nearly the frequency f_1, in our case. It has a value of approximately 2.1 at 3350 MHz and 1.2 at 7100 MHz, which are the two frequencies of interest to us here.

Once the slot frequency f_s has been calculated from the slot dimensions, it is divided by the measured value of the cavity frequency f_1 to give the parameter ω_s/ω_1.

The other coupling parameter, L_s/L_1, is not so readily calculated from the resonator dimensions. The value of the inductance L_s could be found from a knowledge of the slot resonant frequency and the ratio L_s/C_s. This latter ratio may in turn be related to the wave admittance of the slot regarded as a transmission line[10,11,12]. However, it is not entirely clear how to relate the value of L_s computed in this way to the value of L_1 calculated from the measured frequency and R_{sh}/Q of the uncoupled cavity of the resonator. It is possible that the correct value of L_s to use could be determined from the ratio L_s/C_s obtained from a direct measurement of the R_{sh}/Q of the slot. However, no attempt has been made to measure either the R_{sh}/Q or the resonant frequency of the slots. Furthermore, there would still be some doubt as to whether the value of L_s was correct since the position within the slot where its R_{sh}/Q was measured would have to be chosen arbitrarily.

Because of the uncertainty mentioned above in how to directly determine the correct value of L_s/L_1 corresponding to a given physical resonator, the value of this parameter actually used in the comparison with experimental cases was chosen as follows. The theoretical slot resonant frequency was computed from either Eq. (21) or Eq. (22), and then L_s/L_1 was adjusted until ω_π/ω_1 as calculated from Eq. (13) was the same or nearly the same as the value of $f_\pi/f_{2\pi}$ in the experimental resonator under comparison. The predicted $(R_{sh}/Q)_\pi$ was then computed from Eq. (18) and compared with the measured value of $(R_{sh}/Q)_\pi$.

Curves showing the variation of the theoretical values of ω_π/ω_1 and $(R_{sh}/Q)_\pi$ as a function of the parameters ω_1/ω_s and L_s/L_1 are plotted in Fig. 22. The value assumed for $(R_{sh}/Q)_1$ in this figure is 100 ohms. It should be noted that the experimentally observed values of $(R_{sh}/Q)_{2\pi}$ are approximately twice the R_{sh}/Q of the uncoupled cavities (in the case of identical cavities), which agrees with Eq. (17).

The cold-test resonators chosen for the theory-experiment comparison are two which were reported on in references 4 and 5. The measured π-mode R_{sh}/Q of these resonators as a function of the frequency separation between the two modes was presented in Fig. 24 of reference 4 and Fig. 8 of reference 5.

The numerical results of the comparison are listed in Table III. The value assumed for $(R_{sh}/Q)_1$ in the theoretical calculations was the value measured for the uncoupled cavities of each resonator. These values were 115 ohms for the first resonator (first three cases in Table III) and 108 ohms for the second resonator (last three cases in Table III). It can be seen that the predicted values of $(R_{sh}/Q)_\pi$ are within 10 percent of the measured values in four out of the six cases where the slot frequency was taken to be the frequency where the slot is one-half wavelength long (f_s calculated from Eq. (21)). The difference between the predicted and measured values is much greater than this in five of the six cases where the slot frequency was calculated from Eq. (22). This is rather surprising since one would expect the predicted results to be

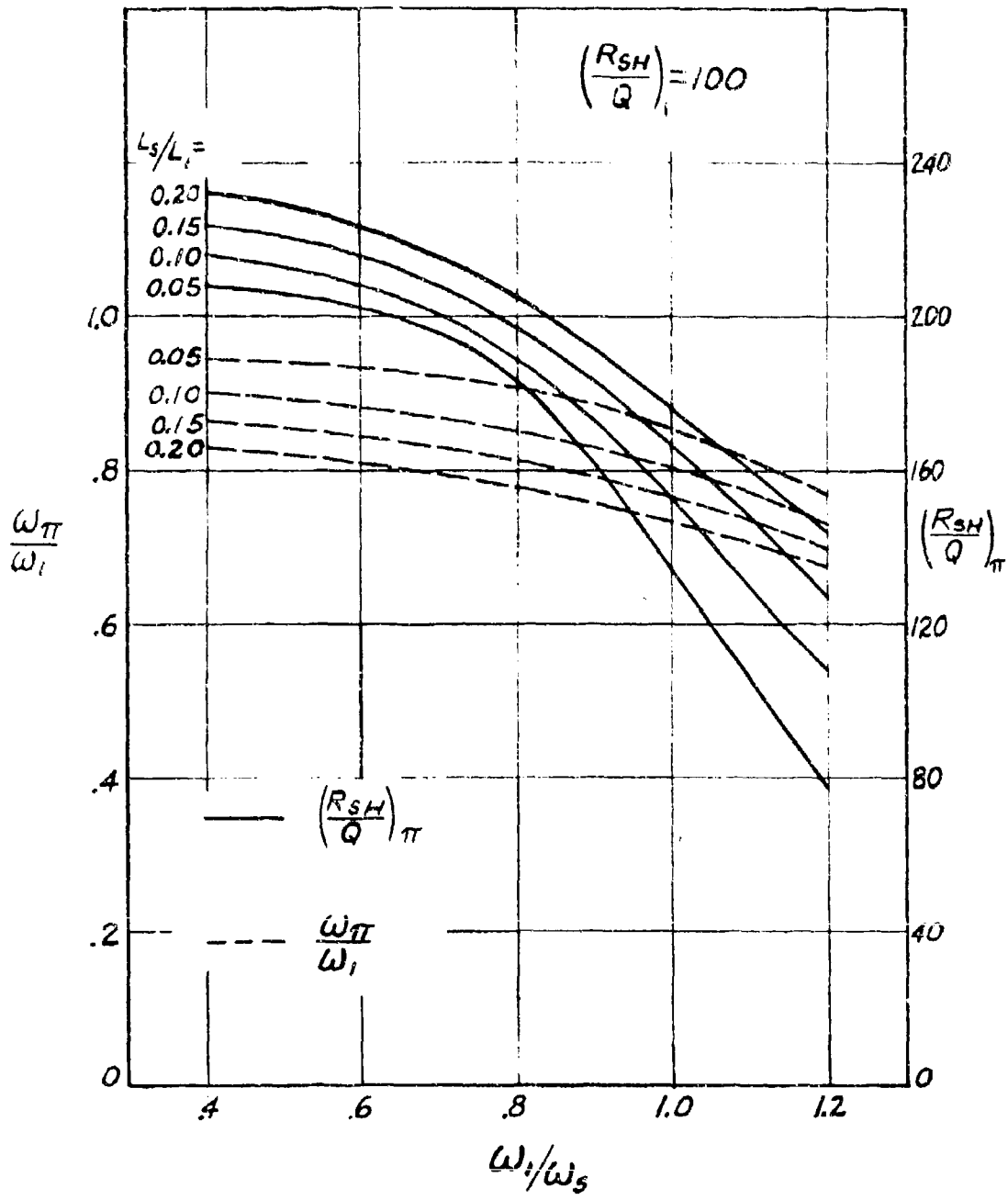

Fig. 22 - Values of ω_π/ω_1 and $(R_{sh}/Q)_\pi$ predicted by the circuit of Fig. 20 as a function of the two coupling parameters ω_1/ω_s and L_s/L_1.

Experimental						Theoretical[1]				Theoretical[2]			
Coupling Slot Dimensions			Measured Values			Input Parameters		Calculated Values		Input Parameters		Calculated Values	
R inches	r inches	θ degrees	f_1 MHz	$f_\pi/f_{2\pi}$	$(R/Q)_\pi$ ohms	f_s/f_1	L_s/L_1	$f_\pi/f_{2\pi}$	$(R/Q)_\pi$ ohms	f_s/f_1	L_s/L_1	$f_\pi/f_{2\pi}$	$(R/Q)_\pi$ ohms
.906	.172	45	3350	.969	212	1.67	.025	.965	230	1.69	.025	.965	230
.906	.172	90	3350	.819	151	1.00	.075	.825	165	1.10	.10	.830	198
.906	.172	110	3350	.731	130	.845	.125	.725	140	.983	.20	.730	201
.480	.172	30	7100	.922	178	1.40	.05	.920	220	1.83	.075	.915	225
.480	.172	60	7100	.809	153	.982	.10	.795	163	1.23	.15	.810	216
.480	.172	75	7100	.752	147	.855	.10	.745	125	1.08	.20	.750	206

1. slot frequency calculated from Eq. (21)
2. slot frequency calculated from Eq. (22)

TABLE III

Comparison between experimental cases and some theoretical predictions of the equivalent circuit shown in Fig. 20.

better when the slot frequency is determined from the more accurate equation, which presumbly is Eq. (22). However, an examination of Fig. 22 does show that the slot resonant frequency must be quite low, near f_1 when L_s/L_1 is small or even less than f_1 if L_s/L_1 is large, in order for the π-mode R_{sh}/Q to be substantially less than twice $(R_{sh}/Q)_1$, as is observed experimentally. Whether this is an indication that the circuit of Fig. 20 does not adequately represent the physical resonator or instead that Eq. (22) is not a good approximation in our case, or both, is not known. In order to answer the question, it would be necessary to measure the slot frequency and possibly also the slot inductance L_s. This has not been done as yet.

C. Second Equivalent Circuit

A method for establishing lumped-element equivalent circuits which correspond closely to the actual geometrical configuration of microwave structures has been described by Curnow[13,14]. Using his techniques, the resonator of Fig. 21 would be represented in the lossless case by the circuit depicted in Fig. 23. The cavity inductance is split into two parts in recognition of the fact that only a fraction k of the circulating current in the cavity is intercepted by the coupling slots. For example, the path of the current in the first cavity which is intercepted by the slots is represented by the inductance L_1/k, and the remainder of this cavity is represented by the inductance $L_1/(1-k)$.

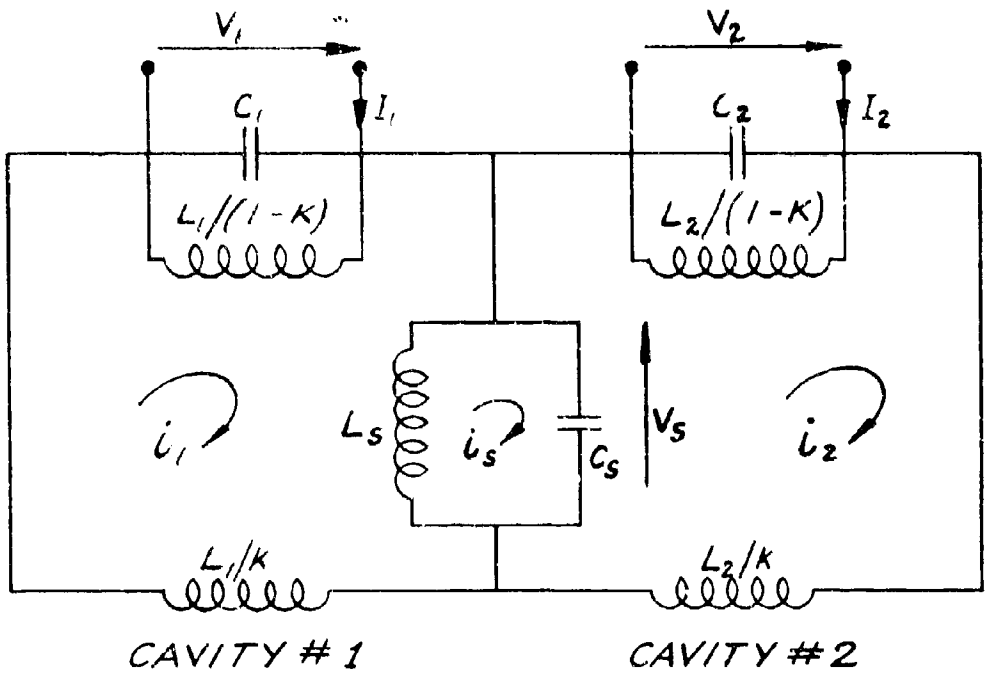

Fig. 23 - A second two-gap resonator equivalent circuit with resonant coupling.

Curnow[14] has shown that this equivalent circuit is more successful than the circuit of Fig. 20 in predicting the dispersion diagram of the long-slot structure, which is basically similar to the cold-test resonators we are concerned with here. It also represents quite well the variation of the Pierce impedance of this structure as a function of the phase shift per section. For these reasons, and also because it more closely represents the geometry of the physical resonator, it was hoped that this circuit would predict the experimentally observed behavior of the π-mode R_{sh}/Q even more accurately than did the previous circuit.

1. Modes of the Lossless Circuit

The characteristic modes of the circuit shown in Fig. 23 were solved for using the same procedure as described for the previous circuit (Fig. 20). Kirchhoff's laws were applied to the circuit, and the resulting equations were solved for the frequencies where i_1, i_2, and i_s are non zero when the two induced gap currents I_1 and I_2 are zero. The two cavities of the resonator were assumed to be identical ($C_1 = C_2$ and $L_1 = L_2$).

This circuit also has three characteristic modes. As before, the two currents i_1 and i_2 are in phase and equal in magnitude at one of the modes. This mode, which corresponds to the observed 2π mode of the cold-test resonator, is at the frequency

$$\omega_a = \omega_{2\pi} = \frac{1}{\sqrt{L_1 C_1}} = \omega_1 \qquad (23)$$

At the other two modes, i_1 and i_2 are equal in magnitude but 180 degrees out of phase. One of these two modes is lower in frequency than ω_1 and therefore corresponds to the measured π mode of the cold-test resonator. Its frequency is

$$\frac{\omega_b}{\omega_1} = \frac{\omega_\pi}{\omega_1} = \left[\frac{2\left[1 + 2k\left(\frac{L_s}{L_1}\right)(1-k)\right]}{1 + 2k\left(\frac{L_s}{L_1}\right) + \left(\frac{\omega_1}{\omega_s}\right)^2 + \sqrt{\left[1 + 2k\left(\frac{L_s}{L_1}\right) + \left(\frac{\omega_1}{\omega_s}\right)^2\right]^2 - 4\left(\frac{\omega_1}{\omega_s}\right)^2\left[1 + 2k\left(\frac{L_s}{L_1}\right)(1-k)\right]}}\right]^{1/2} \tag{24}$$

Note that Eq. (24) reduces to Eq. (13) when k is unity, as it should since the circuit of Fig. 23 becomes the circuit of Fig. 20 when k = 1.

The frequency ω_c of the other π mode can be found from Eq. (24) by replacing the plus sign in front of the radical in the denominator by a minus sign.

2. R_{sh}/Q of the Circuit

The R_{sh}/Q of this circuit was defined the same as in the case of the previous circuit. The expressions for the circuit R_{sh}/Q at the two modes of the resonator were found by evaluating Eqs. (14), (15), and (16) at the two frequencies $\omega_a = \omega_{2\pi}$ and $\omega_b = \omega_\pi$ given above. The results are

$$\left(\frac{R_{sh}}{Q}\right)_{2\pi} = 2\left(\frac{R_{sh}}{Q}\right)_1 \tag{25}$$

$$\left(\frac{R_{sh}}{Q}\right)_\pi = \frac{2\,(R_{sh}/Q)_1}{\frac{\omega_\pi}{\omega_1}\left[1 + \frac{2\left(\frac{\omega_\pi}{\omega_1}\right)^2 \frac{L_s}{L_1}\left[(1-k)\left(\frac{\omega_1}{\omega_\pi}\right)^2 - 1\right]^2}{\left(\frac{\omega_s}{\omega_\pi}\right)^2\left[1 - \left(\frac{\omega_\pi}{\omega_s}\right)^2\right]^2}\right]} \tag{26}$$

where, as before, $(R_{sh}/Q)_1$ is the R_{sh}/Q of the uncoupled cavity of the resonator, and is still related to ω_1 and C_1 by Eq. (19). Eq. (26) reduces to Eq. (18) when k is unity.

3. Comparison with Experimental Cases

The R_{sh}/Q predictions of this circuit were also compared with the measured values listed in Table III. As before, the slot frequencies used in the computation of ω_π and then $(R_{sh}/Q)_\pi$ were calculated from both Eq. (21) and Eq. (22). Initially, the value of the factor k used in each case was taken to be the actual circumferential fraction of the wall between the cavities that was taken up by the coupling slots. As was done with the previous circuit, the parameter L_s/L_1 was adjusted until the calculated value of ω_π/ω_1 agreed with the experimental value of $f_\pi/f_{2\pi}$. The theoretical π-mode R_{sh}/Q was then computed and compared with the cold-test values.

In every instance, the predicted value of $(R_{sh}/Q)_\pi$ was much too high and in many cases was greater than $(R_{sh}/Q)_{2\pi}$, which is contrary to experiment. In order for the theoretical π-mode

R_{sh}/Q given by this circuit to be reasonably close to the experimental values, k would have to be assumed considerably larger than the actual geometrical value. It is difficult to conceive of a physical reason why this should be true. Because of the lack of success initially encountered with this circuit, the investigation into its properties was terminated.

D. Conclusions

The equivalent circuit which should be selected for the theoretical analysis of extended-interaction resonators with mode overlapping is the one which is the simplest and yet adequately represents the physical resonators. The circuit of Fig. 1 is the simplest of the three described in this report, and its single shunt coupling inductance does simulate very well the behavior of the frequencies of the two resonator modes as a function of the coupling between the two cavities. However, as observed previously, this circuit predicts a higher value of the π-mode R_{sh}/Q than the 2π-mode R_{sh}/Q, which is contrary to experiment. This leads to an uncertainty in how to relate the circuit capacitance values to measured quantities in an actual resonator if the circuit is to correctly predict the magnitude of the resonator interaction impedance.

The two equivalent circuits shown in Fig. 20 and Fig. 23 are more complex than the previous circuit, but they do predict $(R_{sh}/Q)_{\pi}$ to be lower than $(R_{sh}/Q)_{2\pi}$ in certain cases. A comparison between these two circuits and measured values from cold-test resonators indicates that the circuit of Fig. 20 comes closest to simulating the

experimental R_{sh}/Q values. However, a final judgement on how well either circuit could represent an actual resonator cannot be made at this time because it is not clear how to relate all of the coupling parameters of these two circuits to physical slot dimensions or to quantities which can be measured in cold test. If this could be done, one of these two circuits would probably be the best choice for resonator synthesis (predicting the individual cavity and coupling slot parameters required to achieve a given overall resonator electrical characteristic) since they more completely describe the coupling slot parameters than does the circuit of Fig. 1. But the circuit of Fig. 1 is still the most efficient circuit to use for the general prediction of the overall resonator behavior as a function of the frequency separation between the two modes, because the other two circuits require a more detailed specification of the slot parameters than is necessary for this type of analysis.

The question still remains as to whether the capacitances of this circuit should be defined in terms of parameters measured at the π-mode frequency or the 2π-mode frequency when the modes overlap. This will best be determined from cold-test measurements of the resonator interaction impedance. Since this cold-test data is not now available, some insight into the answer to this question was gained by computing the interaction impedance of the circuit of Fig. 20 in the driven case and comparing the results with a similar case computed from the circuit of Fig. 1. The circuit of Fig. 20 was chosen to be the "standard of comparison" because it does predict the measured relationship between the π-mode R_{sh}/Q and the 2π-mode

R_{sh}/Q fairly well in some cases, and it was the best circuit available to us from this standpoint.

The circuit parameters assumed for the calculation were selected so the results could be meaningfully compared with the curve of Fig. 14 for which $\gamma_2 = 1.0$. (The impedance represented by this latter curve was calculated from the circuit of Fig. 1, and the circuit capacitances were based on resonator parameters assumed to be measured at the frequency of the uncoupled cavities, which is very nearly the 2π-mode frequency.) The coupling parameters ω_s/ω_1 and L_s/L_1 were chosen to give the same frequency separation between the two modes in the lossless case as in the lossless circuit of Fig. 1 with $\alpha = 0.13$ and $\gamma_2 = 1.0$. The second cavity was then assumed to be loaded to a Q of five and the interaction impedance was computed from Eq. (I-29), as before.

There are a large number of combinations of ω_s/ω_1 and L_s/L_1 which will give the desired mode separation in the lossless case. The computed power output (proportional to the real part of the interaction impedance) for two of these combinations is shown in Figs. 24 and 25. The synchronization between the beam and the circuit (specified by θ_2) was adjusted in each case to yield approximately equal impedances in the two modes. The values of θ_2 differ slightly from that assumed in the curve of Fig. 14, which is plotted as the dashed curve for direct comparison.

The important information to be gathered from these two figures is that in both instances the magnitude of the impedance predicted by the circuit of Fig. 20 is very close to the magnitude of the

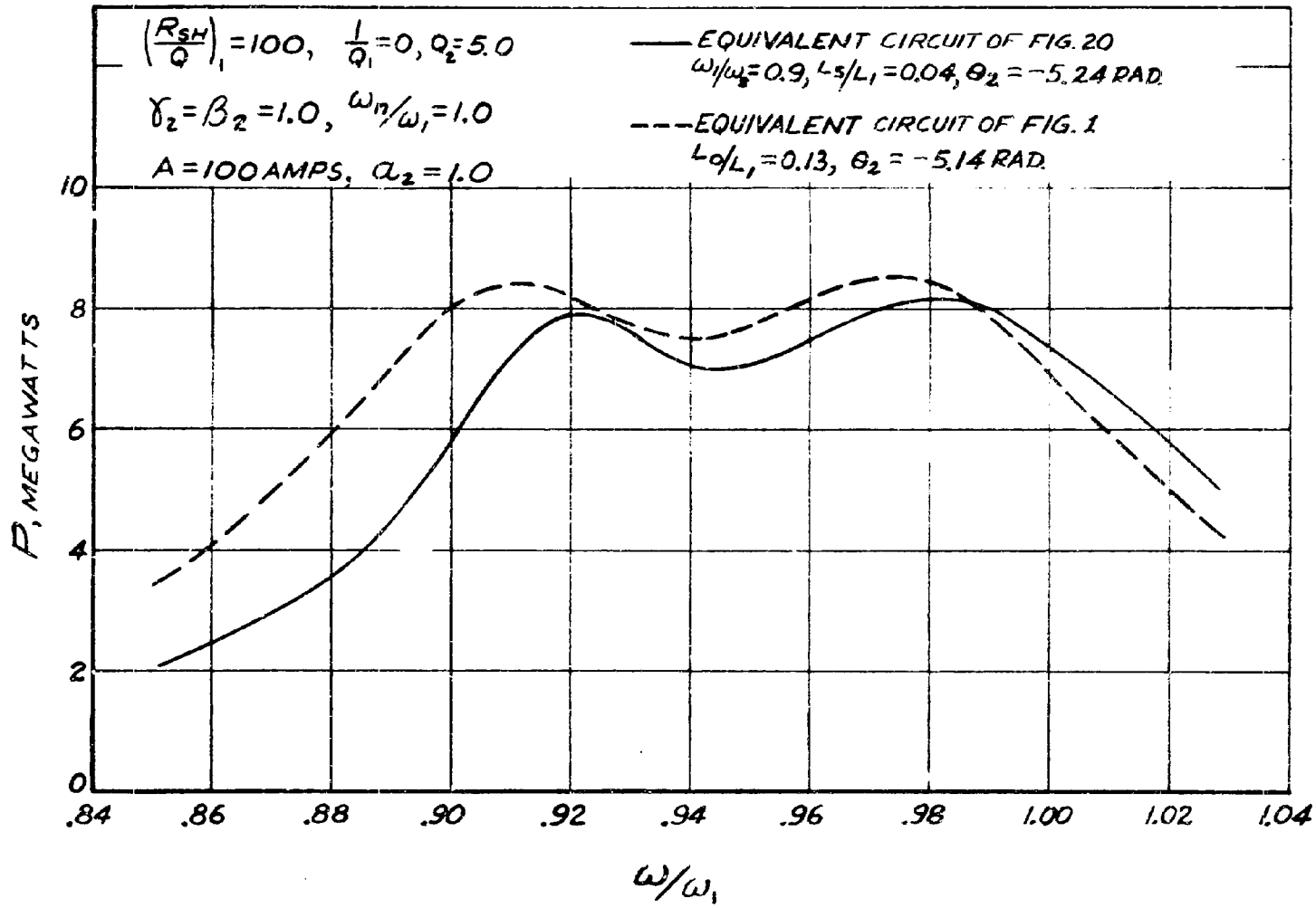

Fig. 24 - Predicted power responses of a driven two-gap resonator as given by two different circuits. The mode separation in the lossless case is the same in both circuits.

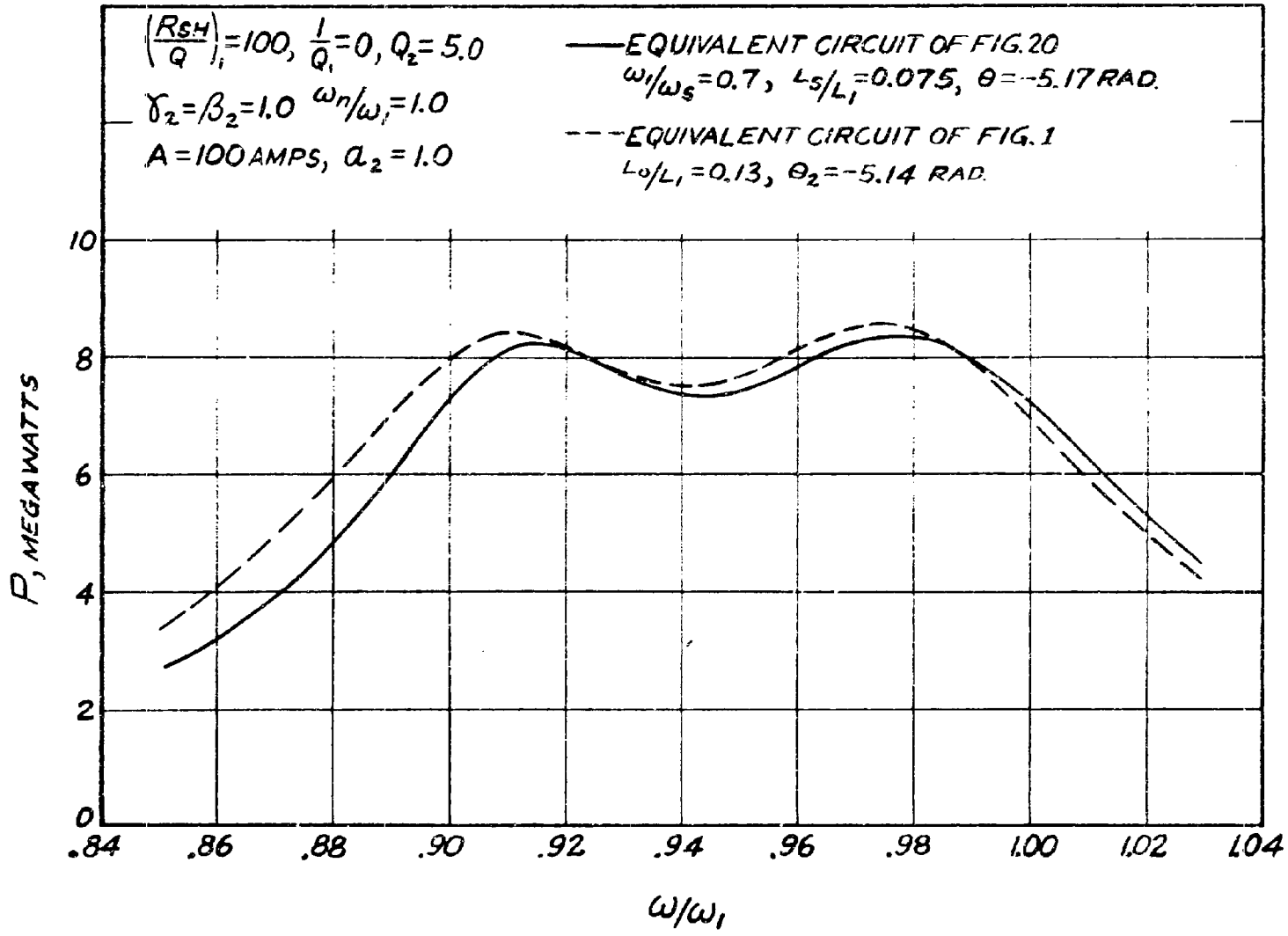

Fig. 25 - A second comparison between the resonator power responses predicted by the two different circuits. The values of ω_1/ω_s and L_s/L_1 have been changed, but the mode separation in the lossless case is still the same as in Fig. 24.

impedance predicted by the circuit of Fig. 1, when the capacitances of this latter circuit were assumed to be based on the value of $(R_{sh}/Q)_1$ measured at ω_1. We have therefore concluded that the circuit capacitances in Fig. 1 should be defined in terms of the measured R_{sh}/Q of the individual uncoupled cavities. It is recognized that before this circuit can be used with complete confidence, its predictions of the interaction impedance of two-gap extended-interaction resonators with mode overlapping will have to be compared with measured values of this impedance. Cold-test techniques which will allow us to perform these measurements will be developed during the next reporting period.

CONCLUSIONS AND FUTURE PLANS

A. Introduction

Throughout the preceding sections of this report, conclusions have been drawn from the results presented. The most significant of these conclusions are reiterated in this section and the proposed direction of future work is described.

B. Conclusions

The characteristic properties of two-gap extended-interaction resonators operating under conditions of mode overlapping have been studied. The most practical resonator model for the analysis is a lumped-element equivalent circuit in which the coupling between the two cavities is represented by a single circuit element.

Computer programs were developed for the calculation of the characteristic modes and the frequency response of the resonators. The influence of the following parameters on the general frequency response of the resonators was established: the coupling between the two cavities, the degree of loading and location of the external load, the beam synchronization parameter, and the relative frequency of the two cavities.

The results show that resonators with mode overlapping can be used for increasing the bandwidth of klystrons. For an interaction impedance in the region of 1800 ohms, the 1 db bandwidth predicted for a two-gap extended-interaction resonator with mode overlapping is approximately a factor three larger than for a two-gap extended-interaction single-mode resonator. The bandwidth advantage over the

single-gap cavity is approximately four to one. The bandwidth is about the same as for the structurally more complex two-gap single-section-filter loaded resonator. However, the frequency response of the resonator with mode overlapping shows a larger sensitivity to the beam voltage than single-mode resonators.

C. Future Plans

The study of extended-interaction resonators with mode overlapping will continue during the next reporting period. In order to provide the necessary tools for further evaluation of the resonators, new analytical as well as cold-test methods must be developed.

A small-signal computer program will be developed for calculating the amplitude and phase response of buncher systems using extended-interaction resonators with mode overlapping. This program will be used for finding the design criteria for buncher systems.

The most straightforward approach to the buncher synthesis is to design each individual buncher resonator with full bandwidth coverage (except for the penultimate resonator system which must be tuned outside the frequency band). The relatively high interaction impedance which can be expected from resonators with mode overlapping indicates that this approach is feasible and will be tried first. The expected small-signal gain per stage is in the region of 10 db.

The development of a large-signal computer program for the final evaluation of output resonators will be started. This program will be capable of simulating and accounting for the remodulation of the beam in the output resonator.

The development of measurement techniques for resonators with mode overlapping will be completed. This is necessary for the cold-test evaluation of both buncher and output resonators. The first step in this work is to establish exactly what information can be obtained from standard impedance measurements where the resonator is excited in the load port. The evaluation of buncher resonators by cold test will be started.

REFERENCES

1. "A Study and Investigation Leading to the Design of Broadband High Power Klystron Amplifiers", U.S. Army Electronics Command Contract No. DA 28-043 AMC 01362(E), June, 1965 - August, 1966.

2. Alain Bert, "Structure de Sortie Pour Klystrons Amplificateurs Formee de Cavities Couplees, A Interaction Multiple", Doctorate Thesis, University of Paris, Paris, France.

3. D. F. Tuttle, Network Synthesis, New York: John Wiley and Sons, Inc., 1958, Vol. 1, p. 716.

4. E. Lien, D. Robinson, "Study and Investigation Leading to the Design of Broadband High Power Klystron Amplifiers", Technical Report No. ECOM-01362-2, January, 1966, pp. 52-57.

5. E. Lien, D. Robinson, "Study and Investigation Leading to the Design of Broadband High Power Klystron Amplifiers", Technical Report No. ECOM-01362-3, July, 1966, pp. 11-17.

6. E. Lien, D. Robinson, "Study and Investigation Leading to the Design of Broadband High Power Klystron Amplifiers", Technical Report No. ECOM-01362-F, November, 1966, p. 57.

7. M. Chodorow, "Recent Progress in High Power Traveling Wave Tubes", Nachrichtentech. Fachber. (NTF), Vol. 22, 1961, pp. 88-93.

8. M. A. Allen, "Coupling of Multiple Cavity Systems", Microwave Lab., W. W. Hansen Labs. of Physics, Stanford University, Stanford, California, M. L. Report No. 584, 1959, p. 99.

9. E. L. Ginzton, Microwave Measurements, New York: McGraw Hill, Inc., 1957, p. 440.

10. A. W. Scott and R. D. Wanselow, "Supporting Research on Beam Interaction Structures for Traveling Wave Tubes", Technical Report No. ASD TR 61-277, January, 1962, pp. 49-55.

11. M. A. Allen, op. cit., pp. 137-139.

12. M. A. Allen and G. S. Kino, "On the Theory of Strongly Coupled Cavity Chains", I.R.E. Trans. on Microwave Theory and Techniques, Vol. MTT-8, May, 1960, pp. 362-372.

13. H. J. Curnow, "A General Equivalent Circuit for Coupled-Cavity Slow-Wave Structures", IEEE Trans. on Microwave Theory and Techniques, Vol. MTT-13, September, 1965, pp. 671-675.

14. H. J. Curnow, "A New Equivalent Circuit for Coupled Cavity Structures", Proc. of the 5th International Congress on Microwave Tubes, Paris: Dunod, 1965, pp. 190-193.

GLOSSARY OF SYMBOLS

a	Drift tube inner radius
a_2	Amplitude coefficient of the current I_2
A	Amplitude of the current I_1
b	Beam radius
c	Velocity of light
C_1, C_2	Equivalent gap capacitances
C_s	Coupling capacitance in the circuits of Fig. 20 and Fig. 23
$\underset{\sim}{C}$	Capacitive reactance matrix, defined by Eq. (1-4)
d	Interaction gap length
$\underset{\sim}{D}$	Normalized capacitance matrix, defined by Eq. (I-21)
f_s	Coupling slot resonant frequency
f_π	π-mode frequency
$f_{2\pi}$	2π-mode frequency
i_1, i_2	Circulating cavity currents, defined in Fig. 1
i_s	Circulating current in the coupling circuits (Fig. 20 and Fig. 23)
$\underset{\sim}{i}$	Circulating cavity current vector
I_1, I_2	Induced gap currents, defined in Fig. 1
$\underset{\sim}{I}$	Induced gap current vector
j	$\sqrt{-1}$
k	The fraction of the circulating cavity current which is intercepted by the coupling slots in a coupled-cavity resonator
$\underset{\sim}{K}$	Impedance matrix, defined by Eq. (I-5)
L_0	Coupling inductance in the circuit of Fig. 1

L_1, L_2	Equivalent cavity inductances
L_s	Coupling inductance in the circuits of Fig. 20 and Fig. 23
$\underset{\sim}{M}$	Normalized impedance matrix, defined by Eq. (I-22)
p	Spacing between the centers of the gaps in an extended-interaction resonator
P	Average power, or real part of $\overline{P}$
$\overline{P}$	Complex power
Q_1, Q_2	Total loaded Q-values of the cavities of a two-gap resonator, measured before the two cavities are coupled together
r	Coupling slot end radius (Fig. 21)
R	Mean coupling slot radius (Fig. 21)
R_1, R_2	Equivalent cavity series resistances
R_{sh}	Cavity shunt resistance
R_{sh}/Q	Cavity characteristic impedance quality factor
u_o	DC beam velocity
U	Stored energy
V	Effective rf resonator voltage
$\underset{\sim}{V}$	RF gap voltage vector
V_1, V_2	RF gap voltages, defined in Fig. 1
Z_0	Reactance of the coupling inductance L_0
Z_1, Z_2	Series cavity impedances, defined by Eq. (I-7) and Eq. (I-11)
Z_{11}, Z_{12}	Elements of the circuit impedance matrix $\underset{\sim}{Z}_c$
Z_{21}, Z_{22}	
Z_c	Resonator interaction impedance
$\underset{\sim}{Z}_c$	Circuit impedance matrix, defined by Eq. (I-15)

α	Coupling parameter associated with the circuit of Fig. 1 ($\alpha = L_o/L_1$)
β_2	L_2/L_1
β_e	Propagation factor associated with the dc beam velocity ($\beta_e = \omega/u_o$)
$\beta_e p$	Normalized spacing between the centers of the gaps in an extended-interaction resonator
γ_2	ω_2/ω_1
θ	Coupling slot angle, defined in Fig. 21
θ_2	Phase of I_2 relative to I_1
σ	Imaginary part of the complex frequency ω' (except in Eq. (23), where σ is an empirical correction factor)
ω	Angular frequency (real part of ω')
ω'	Complex angular frequency
ω_1, ω_2	Angular resonant frequencies of the two resonator cavities before they are coupled together
ω_a, ω_b, ω_c	Angular frequencies of the three characteristic modes of the circuits of Fig. 20 and Fig. 23, in the lossless case
ω_n	Angular frequency of the nth mode
ω_s	Coupling slot angular resonant frequency
ω_π	Angular π-mode frequency
$\omega_{2\pi}$	Angular 2π-mode frequency

APPENDIX I

DERIVATION OF THE BASIC EQUATIONS USED IN THE ANALYSIS OF TWO-GAP EXTENDED-INTERACTION RESONATORS

A. CIRCUIT IMPEDANCE MATRIX

The lumped-element equivalent circuit used to represent two-gap extended-interaction resonators is shown in Fig. 1, page 6. Applying Kirchhoff's laws to the circuit and writing the resulting equations in matrix form, we obtain

$$\underset{\sim}{K}\,\underset{\sim}{i} = \underset{\sim}{C}\,\underset{\sim}{I} \tag{I-1}$$

where

$$\underset{\sim}{I} = \begin{bmatrix} I_1 \\ I_2 \end{bmatrix} \tag{I-2}$$

$$\underset{\sim}{i} = \begin{bmatrix} i_1 \\ i_2 \end{bmatrix} \tag{I-3}$$

$$\underset{\sim}{C} = \frac{-j}{\omega} \begin{bmatrix} 1/C_1 & 0 \\ 0 & 1/C_2 \end{bmatrix} \tag{I-4}$$

$$\underset{\sim}{K} = \begin{bmatrix} (Z_1 + Z_o), & -Z_o \\ -Z_o, & (Z_2 + Z_o) \end{bmatrix} \qquad \text{(I-5)}$$

Z_o is the reactance of the coupling inductance, and Z_1 and Z_2 are the series impedances of the first and second cavities, respectively:

$$Z_o = j\omega L_o \qquad \text{(I-6)}$$

$$Z_1 = R_1 + j\left(\omega L_1 - \frac{1}{\omega C_1}\right) \qquad \text{(I-7)}$$

or

$$Z_1 = j\omega L_1 \left[1 - \left(\frac{\omega_1}{\omega}\right)^2 - j\,\frac{\omega_1}{\omega}\,\frac{1}{Q_1}\right] \qquad \text{(I-8)}$$

where

$$\omega_1^2 = \frac{1}{L_1 C_1} \qquad \text{(I-9)}$$

and

$$Q_1 = \frac{\omega_1 L_1}{R_1} \qquad \text{(I-10)}$$

similarly

$$Z_2 = j\omega L_2 \left[1 - \left(\frac{\omega_2}{\omega}\right)^2 - j\,\frac{\omega_2}{\omega}\,\frac{1}{Q_2}\right] \qquad \text{(I-11)}$$

It is easy to show that the gap voltage vector $\underset{\sim}{V}$ is related to the two current vectors and the gap capacitance matrix through the equation

$$\underset{\sim}{V} = \underset{\sim}{C}\,(\underset{\sim}{I} - \underset{\sim}{i}) \tag{I-12}$$

where

$$\underset{\sim}{V} = \begin{bmatrix} V_1 \\ V_2 \end{bmatrix} \tag{I-13}$$

Combining Eqs (I-1) and (I-12), we obtain:

$$\underset{\sim}{V} = \underset{\sim}{C}\,\underset{\sim}{I} - \underset{\sim}{C}\,\underset{\sim}{K}^{-1}\,\underset{\sim}{C}\,\underset{\sim}{I} \tag{I-14}$$

We have defined the circuit impedance matrix $\underset{\sim}{Z}_c$ to be

$$\underset{\sim}{Z}_c = \underset{\sim}{C} - \underset{\sim}{C}\,\underset{\sim}{K}^{-1}\underset{\sim}{C} \tag{I-15}$$

which yields the relationship

$$\underset{\sim}{V} = \underset{\sim}{Z}_c\,\underset{\sim}{I} \tag{I-16}$$

It is useful to write the expression for $\underset{\sim}{Z}_c$ in a slightly different form by using the parameters of cavity #1 as a reference.

Using ω_1 and L_1 for reference in Eq (I-11), Z_2 becomes

$$Z_2 = j\omega L_1\,\beta_2\left[1 - \gamma_2^2\left(\frac{\omega_1}{\omega}\right)^2 - j\,\frac{\omega_1}{\omega}\,\frac{\gamma_2}{Q_2}\right] \tag{I-17}$$

where

$$\beta_2 = \frac{L_2}{L_1} \tag{I-18}$$

and

$$\gamma_2 = \frac{\omega_2}{\omega_1} \tag{I-19}$$

With Z_2 given by Eq (I-17), $\underset{\sim}{Z}_c$ can be expressed as

$$\underset{\sim}{Z}_c = -\frac{j}{\omega C_1}\left[\underset{\sim}{D} + \left(\frac{\omega_1}{\omega}\right)^2 \underset{\sim}{D}\,\underset{\sim}{M}^{-1}\,\underset{\sim}{D}\right] \tag{I-20}$$

where

$$\underset{\sim}{D} = j\omega C_1\,\underset{\sim}{C} \tag{I-21}$$

and

$$\underset{\sim}{M} = \frac{1}{j\omega L_1}\,\underset{\sim}{K} \tag{I-22}$$

In an ordinary R-L-C circuit, such as we are using to represent cavity #1 or cavity #2 in Fig. 1, the ratio of the equivalent shunt resistance to the circuit Q (R_{sh}/Q) can be expressed as the reciprocal of the product of the circuit capacitance and resonant frequency. In order to relate the capacitances in our equivalent circuit to a particular two-gap resonator operating in some given mode, we have chosen to define the capacitances C_1 and C_2 in terms of the measured R_{sh}/Q of the resonator at the given mode and the mode frequency. So, for example,

$$\frac{1}{C_1} = \omega_n \left(\frac{R_{sh}}{Q}\right)_1 \tag{I-23}$$

where ω_n is the angular frequency of the mode of interest. In the most common case where the resonator gaps are identical, $(R_{sh}/Q)_1$ is taken to be one half the measured R_{sh}/Q of the overall resonator for that mode.

Substituting Eq (I-23) into Eq (I-20), the final expression for the circuit impedance matrix becomes

$$\underset{\sim}{Z}_c = -j\left(\frac{R_{sh}}{Q}\right)_1 \frac{\omega_n}{\omega}\left[\underset{\sim}{D} + \left(\frac{\omega_1}{\omega}\right)^2 \underset{\sim}{D}\,\underset{\sim}{M}^{-1}\,\underset{\sim}{D}\right] \qquad \text{(I-24)}$$

B. Resonator Interaction Impedance

We have chosen to define the interaction impedance of the resonator in terms of the power delivered to the resonator for a specified current excitation of the resonator. The complex power delivered to the resonator is given by

$$\bar{P} = \frac{1}{2}\,\tilde{V}\,\underset{\sim}{I}^* \qquad \text{(I-25)}$$

where $\tilde{V}$ is the transpose of the column vector $\underset{\sim}{V}$, the asterisk indicates complex conjugate, and the bar over the P is used to indicate that the power as defined here is complex.

Using the induced current in the first gap as a reference, the most general expression for the current vector $\underset{\sim}{I}$ is

$$\underset{\sim}{I} = \begin{bmatrix} I_1 \\ I_2 \end{bmatrix} = A \begin{bmatrix} 1 \\ a_2 e^{j\,\theta_2} \end{bmatrix} \qquad \text{(I-26)}$$

The voltage vector is related to the circuit impedance matrix and the current vector by

$$\underset{\sim}{V} = \underset{\sim}{Z}_c \, \underset{\sim}{I} = \begin{bmatrix} Z_{11} & Z_{12} \\ Z_{21} & Z_{22} \end{bmatrix} \begin{bmatrix} I_1 \\ I_2 \end{bmatrix} \tag{I-27}$$

Substituting Eqs (I-26) and (I-27) into Eq (I-25), and recognizing that $Z_{21} = Z_{12}$ since the resonator is passive, the expression for the complex power becomes

$$\overline{P} = \frac{A^2}{2} \left[Z_{11} + a_2^2 \, Z_{22} + 2a_2 \, Z_{12} \cos \theta_2 \right] \tag{I-28}$$

The resonator interaction impedance is defined to be

$$Z_c = \frac{2\overline{P}}{A^2} \tag{I-29}$$

so

$$Z_c = Z_{11} + a_2^2 \, Z_{22} + 2a_2 \, Z_{12} \cos \theta_2 \tag{I-30}$$

The power dissipated in the resonator and its associated external load is just the real part of the complex power. That is,

$$P = \frac{1}{2} \operatorname{Re} \left(\tilde{V} \, \underset{\sim}{I}^* \right) = \frac{A^2}{2} \operatorname{Re} Z_c \tag{I-31}$$

C. <u>Frequencies and Q's of the Characteristic Resonator Modes</u>

The characteristic mode frequencies of the resonator are

defined to be the frequencies for which the voltage vector $\underset{\sim}{V}$ is non zero when there is no external excitation of the resonator ($\underset{\sim}{I} = 0$). When $\underset{\sim}{I} = 0$, Eqs (I-1) and (I-12) become

$$\underset{\sim}{K}\,\underset{\sim}{i} = 0 \tag{I-32}$$

and

$$\underset{\sim}{V} = -\,\underset{\sim}{C}\,\underset{\sim}{i} \tag{I-33}$$

Barring the cases where either the frequency or the circuit capacitances are infinite, Eq (I-33) shows that for $\underset{\sim}{V}$ to be non zero, $\underset{\sim}{i}$ must be non zero. With that being true, Eq (I-32) is satisfied only if the determinant of the K matrix is zero

$$\left|\underset{\sim}{K}\right| = 0 \tag{I-34}$$

Only in the lossless case can this last equation be satisfied at real frequencies. In the cases with loss, the characteristic modes are found by solving for the complex frequencies

$$\omega' = \omega + j\,\sigma \tag{I-35}$$

which are the roots of Eq (I-34).

The Q of each mode of the undriven resonator can be found from the complex frequency corresponding to that mode. The Q is given by[3]

$$Q = \frac{\omega}{2\sigma} \tag{I-36}$$

D. Gap Voltages at the Modes of the Undriven Resonator

Combining Eqs (I-1) and (I-12) when $\underset{\sim}{I} = 0$ yields the equation

$$\underset{\sim}{K}\,\underset{\sim}{C}^{-1}\,\underset{\sim}{V} = 0 \qquad \text{(I-37)}$$

This equation can be used to find the phase and amplitude of V_2 relative to V_1 at the modes of the undriven resonator by evaluating it at the complex frequency roots of Eq (I-34).

UNCLASSIFIED

Security Classification

DOCUMENT CONTROL DATA - R&D

(Security classification of title, body of abstract and indexing annotation must be entered when the overall report is classified)

1. ORIGINATING ACTIVITY (Corporate author) VARIAN ASSOCIATES San Carlos, California	2a. REPORT SECURITY CLASSIFICATION UNCLASSIFIED 2b. GROUP N/A

3. REPORT TITLE

BROADBAND, HIGH POWER KLYSTRON AMPLIFIER

4. DESCRIPTIVE NOTES (Type of report and inclusive dates)

First Tri-Annual - 10 Aug - 9 Dec 66

5. AUTHOR(S) (Last name, first name, initial)

Lien E.; Robinson D.

6. REPORT DATE March 1967	7a. TOTAL NO. OF PAGES 72	7b. NO. OF REFS
8a. CONTRACT OR GRANT NO. DA 28-043 AMC-02157 (E) b. PROJECT NO. 1E6-22001-A-055-04-78 c. d.	9a. ORIGINATOR'S REPORT NUMBER(S) 9b. OTHER REPORT NO(S) (Any other numbers that may be assigned this report) ECOM-02157-1	

10. AVAILABILITY/LIMITATION NOTICES

This document is subject to special export controls and each transmittal to foreign governments or foreign nationals may be made only with prior approval of CG, USAECOM, ATTN: AMSEL-KL-TM, Fort Monmouth, New Jersey 07703.

11. SUPPLEMENTARY NOTES	12. SPONSORING MILITARY ACTIVITY U. S. Army Electronics Command Fort Monmouth, New Jersey AMSEL-KL-TM

13. ABSTRACT The purpose of this program is to investigate methods for improving the bandwidth capabilities of high-power klystron amplifiers. The objective is a 1 db bandwidth improvement of at least fifty percent over the current state of the art. Particular emphasis is being placed on the study of extended-interaction resonators, and the possible optimization of these resonators through the use of mode overlapping.

In this report, the results of the initial investigation into the effects of mode overlapping in extended-interaction resonators is presented. During the first four-month reporting period, this investigation has been primarily concerned with the influence of a number of different parameters on the interaction impedance, bandwidth, and frequency response of the resonators. The parameters of particular interest are the coupling between the two cavities, the degree of external loading and the location of the external load, the beam synchronization parameter, and the relative frequencies of the two cavities. The initial analysis has been restricted to two-gap resonators.

It is shown theoretically that the bandwidth of extended-interaction resonators can be increased through the use of mode overlapping. Comparisons with the bandwidths of other types of resonators at a given maximum impedance level show that a two-gap extended-interaction resonator with mode overlapping can have a 1 db bandwidth advantage of approximately three to one over a two-gap, single-mode, extended-interaction resonator, and close to four to one over a conventional single-gap cavity. The bandwidth of a two-gap, single-section-filter loaded resonator is about the same as that of the two-gap, mode-overlapping resonator at a given impedance level.

DD FORM 1 JAN 64 1473

UNCLASSIFIED

Security Classification

Security Classification

14. KEY WORDS	LINK A ROLE	LINK A WT	LINK B ROLE	LINK B WT	LINK C ROLE	LINK C WT

INSTRUCTIONS

1. ORIGINATING ACTIVITY: Enter the name and address of the contractor, subcontractor, grantee, Department of Defense activity or other organization *(corporate author)* issuing the report.

2a. REPORT SECURITY CLASSIFICATION: Enter the overall security classification of the report. Indicate whether "Restricted Data" is included. Marking is to be in accordance with appropriate security regulations.

2b. GROUP: Automatic downgrading is specified in DoD Directive 5200.10 and Armed Forces Industrial Manual. Enter the group number. Also, when applicable, show that optional markings have been used for Group 3 and Group 4 as authorized.

3. REPORT TITLE: Enter the complete report title in all capital letters. Titles in all cases should be unclassified. If a meaningful title cannot be selected without classification, show title classification in all capitals in parenthesis immediately following the title.

4. DESCRIPTIVE NOTES: If appropriate, enter the type of report, e.g., interim, progress, summary, annual, or final. Give the inclusive dates when a specific reporting period is covered.

5. AUTHOR(S): Enter the name(s) of author(s) as shown on or in the report. Enter last name, first name, middle initial. If military, show rank and branch of service. The name of the principal author is an absolute minimum requirement.

6. REPORT DATE: Enter the date of the report as day, month, year; or month, year. If more than one date appears on the report, use date of publication.

7a. TOTAL NUMBER OF PAGES: The total page count should follow normal pagination procedures, i.e., enter the number of pages containing information.

7b. NUMBER OF REFERENCES: Enter the total number of references cited in the report.

8a. CONTRACT OR GRANT NUMBER: If appropriate, enter the applicable number of the contract or grant under which the report was written.

8b, 8c, & 8d. PROJECT NUMBER: Enter the appropriate military department identification, such as project number, subproject number, system numbers, task number, etc.

9a. ORIGINATOR'S REPORT NUMBER(S): Enter the official report number by which the document will be identified and controlled by the originating activity. This number must be unique to this report.

9b. OTHER REPORT NUMBER(S): If the report has been assigned any other report numbers *(either by the originator or by the sponsor)*, also enter this number(s).

10. AVAILABILITY/LIMITATION NOTICES: Enter any limitations on further dissemination of the report, other than those imposed by security classification, using standard statements such as:

(1) "Qualified requesters may obtain copies of this report from DDC."

(2) "Foreign announcement and dissemination of this report by DDC is not authorized."

(3) "U. S. Government agencies may obtain copies of this report directly from DDC. Other qualified DDC users shall request through _____."

(4) "U. S. military agencies may obtain copies of this report directly from DDC. Other qualified users shall request through _____."

(5) "All distribution of this report is controlled. Qualified DDC users shall request through _____."

If the report has been furnished to the Office of Technical Services, Department of Commerce, for sale to the public, indicate this fact and enter the price, if known.

11. SUPPLEMENTARY NOTES: Use for additional explanatory notes.

12. SPONSORING MILITARY ACTIVITY: Enter the name of the departmental project office or laboratory sponsoring *(paying for)* the research and development. Include address.

13. ABSTRACT: Enter an abstract giving a brief and factual summary of the document indicative of the report, even though it may also appear elsewhere in the body of the technical report. If additional space is required, a continuation sheet shall be attached.

It is highly desirable that the abstract of classified reports be unclassified. Each paragraph of the abstract shall end with an indication of the military security classification of the information in the paragraph, represented as *(TS)*, *(S)*, *(C)*, or *(U)*.

There is no limitation on the length of the abstract. However, the suggested length is from 150 to 225 words.

14. KEY WORDS: Key words are technically meaningful terms or short phrases that characterize a report and may be used as index entries for cataloging the report. Key words must be selected so that no security classification is required. Identifiers, such as equipment model designation, trade name, military project code name, geographic location, may be used as key words but will be followed by an indication of technical context. The assignment of links, rules, and weights is optional.

Security Classification